LICENTIATE THESIS

High Performing Cast Aluminium-Silicon Alloys

Martin I. Riestra Perna

JÖNKÖPING UNIVERSITY
School of Engineering

Department of Materials and Manufacturing

SCHOOL OF ENGINEERING, JÖNKÖPING UNIVERSITY

Jönköping, Sweden 2017

Licentiate Thesis

High Performing Cast Aluminium-Silicon alloys

Martin I. Riestra Perna

Department of Materials and Manufacturing
School of Engineering, Jönköping University
SE-551 11 Jönköping, Sweden
Martin.riestra@ju.se

Research Series from the School of Engineering, Jönköping University
Department of Materials and Manufacturing
Dissertation Series No. 33, 2017
ISBN: 978-91-87289-34-7

Published and Distributed by
School of Engineering, Jönköping University
Department of Materials and Manufacturing
SE-551 11 Jönköping, Sweden

Printed in Sweden by
Ineko AB
Kållered, 2017

ABSTRACT

The need to produce lighter components due to environmental aspects and the development of electrical vehicles represents an opportunity for cast aluminium-silicon alloys. With high specific strength, good castability, high corrosion resistance and recyclability, these alloys offer an attractive combination of properties as an alternative to steel, cast iron and titanium-based components in certain applications. To take advantage of such a combination of properties, there is a need to ensure that they can be reliably achieved. In other words, high performing components need to be produced. For that, the production cycle, from alloy selection and melt preparation, to the casting and heat treatment of the component must be understood and controlled as a whole. The different steps in the production cycle will affect the microstructure of the components and hence the resulting mechanical properties. Understanding the relation between the different steps in the production cycle, its consequences on the microstructural features and on the mechanical properties constitutes the aim of this thesis.

Experiments applying state-of-the-art knowledge regarding effect of casting process, alloying system and post-process variables were performed aimed at achieving properties similar to those of high pressure die casting (HPDC) components. Different melt quality determination tools were evaluated on three different EN AC-46000 melt qualities. The influence of modification, grain refinement and both treatments together was assessed on an Al-10Si alloy solidified under different cooling rates. The tensile behaviour and the impact of features such as secondary dendrite arm spacing (SDAS) or grain sizes was quantified.

It was corroborated that by appropriate selection and control of such alloying system, process and post-process variables it is possible to achieve HPDC EN AC-46000 tensile and fatigue properties through a T5 treated sand cast EN AC-42100 alloy. On the other hand, the available techniques for melt quality assessment are inadequate, requiring further analysis to successfully identify the melt quality. Additionally, it was observed that decreasing the melt quality by additions of 25 wt.% of machining chips did not significantly decrease the tensile properties but slightly increased the variation in them. In relation to the modification and grain refinement of Al-10Si alloys it was concluded that with the slowest cooling rate tested, additions of only grain refiner did not successfully produce equiaxed grains. For cooling rates corresponding to dendrite arm spacings of 15 μm and slower, combined additions of grain refiner and modifier can lead to higher tensile properties compared to the corresponding separate additions. SDAS was observed to describe flow stress through the Hall-Petch equation but grain size did not show a physically meaningful relationship. Furthermore, beginning of cracking was detected in the plastic deformation region at dendrite/eutectic boundaries and propagated in a trans-granular fashion.

Keywords: Aluminium cast alloys, melt quality, eutectic modification, grain refinement, microstructure, tensile properties

ACKNOWLEDGEMENTS

I would like to express my sincere gratitude to:

Salem Seifeddine for being my supervisor, for his support, guidance, trust and for this and all the opportunities he has given me.

Ehsan Ghassemali for being my supervisor, for his valuable comments and corrections and for the suggestions given.

Toni Bogdanoff for his help and support in experimental work, his endless curiosity, for sharing his ideas with me and for being a fun travel companion.

Juan Carlos Hernando for his friendship and advice, his altruistic help and support and for the endless hours of discussion.

All my colleagues and friends at the department of Materials and Manufacturing and School of Engineering, for the enjoyable conversations, the breakfasts laughs and jokes along the years.

The Region Jönköpings Län and Jönköping University for the financial support of the HINT project.

The industrial partners Fagerhult Belysning AB, Lundbergs Pressgjuteri AB, Ventana Hackås (Foundry Division) and Bryne AB for their valuable support and contribution.

To Sebastian Wachauf-Tautermann for putting up with me all these years, for his help and support, fruitful discussions and advice.

To my beloved family for their love, support, advice, endless jokes and just for being there. Especially to Judit for sharing this road with me, for her patience, inspiration and support.

Martin I. Riestra Perna

Jönköping, October 2017

SUPPLEMENTS

The following supplements constitute the basis of this thesis:

Supplement I

M. Riestra, S. Seifeddine, E. Sjölander; Tailoring Al-7Si-0.3Mg Cast Alloy Properties to Represent HPDC Tensile and Fatigue Behaviour in Component Prototypes.

Presented in High Tech Die Casting 2016, June 22nd-23rd, Venice, Italy. Published in Metallurgia Italiana, Associazione Italiana di Metallurgia. (2016) **108**: pp. 33-36.

M. Riestra was the main author. S. Seifeddine and E. Sjölander contributed with advice regarding the work.

Supplement II

M. Riestra, A. Bjurenstedt, T. Bogdanoff, E. Ghassemali, S. Seifeddine; Complexities in the Assessment of Melt Quality.

Presented in MS&T17, Light Metals Technology 2017, October 8th-12th, Pittsburgh, Pennsylvania, USA. Published in International Journal of Metalcasting 2017, DOI 10.1007/s40962-017-0179-y.

M. Riestra was the main author. A. Bjurenstedt and T. Bogdanoff designed and assisted during experimental work, analysis of results and advice regarding the work. E. Ghassemali and S. Seifeddine contributed with advice regarding the work.

Supplement III

M. Riestra, E. Ghassemali, T. Bogdanoff, S. Seifeddine; Interactive Effects of Grain Refinement, Eutectic Modification and Solidification Rate on Tensile Properties of Al-10Si Alloy.

Materials Science and Engineering: A, 2017. **703**: p. 270-279

M. Riestra was the main author. E. Ghassemali assisted with EBSD analysis and advice regarding the work. T. Bogdanoff assisted during experimental work, analysis of results and advice regarding the work. S. Seifeddine contributed with advice regarding the work.

Supplement IV

E. Ghassemali, M. Riestra, T. Bogdanoff, B.S. Kumar, S. Seifeddine; Hall-Petch Equation in a Hypoeutectic Al-Si Cast Alloy: Grain Size vs. Secondary Dendrite Arm Spacing.

To be published in Procedia Engineering.

E. Ghassemali was the main author; together with M. Riestra, they designed and performed the investigation. T. Bogdanoff and B.S. Kumar assisted during experimental work. S. Seifeddine contributed with advice regarding the work.

TABLE OF CONTENTS

CHAPTER I

INTRODUCTION

CHAPTER INTRODUCTION

The variables governing the performance of cast aluminium alloys are presented along with relevant concepts and phenomena. It follows with a description of the means to control the resulting microstructures and therefore the mechanical properties.

1.1 BACKGROUND

Aluminium has become a lightweight alternative to traditionally used metals such as steel, cast iron or titanium. In applications where increasing demands related to emissions, consumer requirements for fuel efficiency or consumption of raw materials, aluminium constitutes an important option as a high specific strength, cost-efficient and recyclable material.

Casting is the most common technique to economically produce complex, near net-shape components in a wide variety of sizes. In it, aluminium along with some other alloying elements is introduced into a mould and is allowed to solidify. The means of introducing the molten metal in the mould and the material the mould is made of determine the different casting techniques, i.e. sand casting, gravity die casting, high pressure die casting (HPDC)…etc.

The performance of the resulting component has been identified to be related to three key sets of variables [1]:

- **System variables**, which include alloying elements selection, chemical compositions, or concepts such as level of modification or grain refinement that will be treated later.
- **Process variables**, which include how the molten metal is treated, the local solidification times in the mould, the manufacturing technique selection, etc.
- **Post-solidification variables**, which include solution heat treatments, quenching, ageing, etc.

By careful selection and control of these sets of variables, the material microstructure can be controlled. Consequently, the resulting properties and the spread in such properties can be improved. The level of rejected castings due to lack of quality or manufacturing issues can be reduced with the corresponding environmental savings. Thus, the performance of the final component can be ensured.

1.2 SYSTEM VARIABLES

1.2.1 Aluminium–Silicon casting alloys

Among the different aluminium alloy systems, the most used is the Aluminium-Silicon (Al-Si) system with Si concentrations in the range of 5 to 23 wt.%. This alloy system has an eutectic point at 12.6 wt.% Si at 577 °C [2] as shown in the phase diagram in Figure 1. Si increases the fluidity of the molten metal, therefore improving the castability. Increased tensile strength, good corrosion resistance as well as machinability are also results of alloying with Si. Depending on the Si content, different structures will form; hypoeutectic, eutectic or hypereutectic. The resulting microstructure is a consequence of the solidification path. Following the phase diagram, hypoeutectic alloys are characterized for having α-Al dendrites solidifying first, surrounded by Al-Si eutectic. Hypereutectic alloys have primary Si particles forming first followed by the Al-Si eutectic. The current work focuses on hypoeutectic alloys.

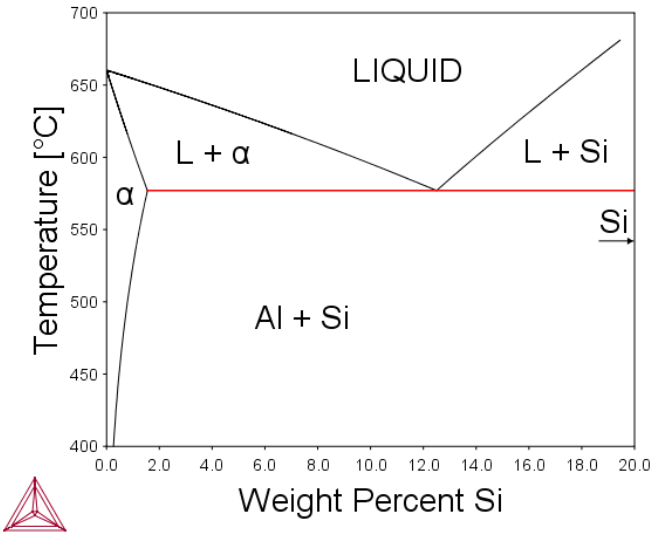

Figure 1. Stable binary Al-Si phase diagram

To further control the properties of the cast parts, other elements can be added.

1.2.2 Alloying elements

In addition to Si, other elements can be present in aluminium alloys. Magnesium (Mg) and copper (Cu) constitute the two more common alloying elements added to increase the strength of the alloys, but they can also lead to a reduction of ductility. Their effect on the properties is dependent on how they are present in the microstructure: as atoms in solid solution, as Guinier-Preston (GP) zones, as fine precipitates or as coarse phases [3].

The addition of Mg results in a strengthening effect in Al-Si alloys by precipitation of Mg_2Si and by transforming the deleterious β-Al_5FeSi platelets that form due to the presence of Fe into a less harmful $Al_8Mg_3FeSi_6$ Chinese script morphology [4]. This transformation will result in an increase of strength for Mg levels up to about 0.5 wt.% and above such level no increase in strength is expected after a T6 treatment [5].

Addition of Cu leads to precipitation of a coarse θ-Al_2Cu phase upon solidification. It can be present either as a massive blocky phase or as a fine eutectic [6]. If, after heat treatment, spheroidised Cu particles in solid solution are distributed homogeneously though the α-Al matrix, an increase in strength will be obtained while retaining substantial ductility [7]. On the other hand, addition of Cu will increase porosity formation. The possible mechanisms explaining this are a decrease in hydrogen solubility and/or the increased solidification range due to a high Cu content in the melt. Because of the increased solidification range, a smaller fraction of binary eutectic is available resulting in a more likely formation of shrinkage porosity [8].

Iron is generally considered an impurity from production of pure aluminium or from recycling. Depending on the alloy composition, especially the Fe level, the melt treatment, the casting conditions and the cooling rate, Fe can appear in different morphologies; β-Al_5FeSi platelets, $Al_{15}(Fe,Mn)_3Si_2$ Chinese scripts and polyhedral and/or star-like crystals [7, 9]. To avoid detrimental effects on ductility and fracture toughness, Fe should be kept as low as pratically possible [10]. Additions of Mn at Mn:Fe ratios of ~ 0.5 have been suggested to reduce β-Fe phase and promote α-Fe phase as it has been traditionally considered to improve ductility [11].

The influence of the different elements in an alloy varies. Phases of diverse shape and size form due to the elements present during solidification. How these phases are present in the microstructure will influence the properties of the cast part. This holds especially true for the Si present in hypoeutectic alloys.

1.2.3 Modification

The process by which flake-like Si is changed into a more fibrous morphology is called modification. There are several ways this can be achieved, the two most common are quench modification and chemical modification. The former can be produced by a rapid solidification, while for the later, elements such as strontium (Sr), sodium (Na) or antimony (Sb) are added to the melt [12]. These elements, referred to as modifiers, are effective at very low concentration levels. Two classes of theories have been proposed to explain the chemical modification effect; the restricted nucleation and the restricted growth theory [13]. Within the restricted growth theory, the *Impurity Induced Twinning* [14] (Figure 3a) explain the impairing of the Si growth by poisoning the growing Si ledges and the *TPRE Poisoning* [15] (Figure 3b) by poisoning the re-entrant edges, stopping the twin plane re-entrant mechanism. The work by Timpel et al. [16] demonstrated that both mechanisms take place.

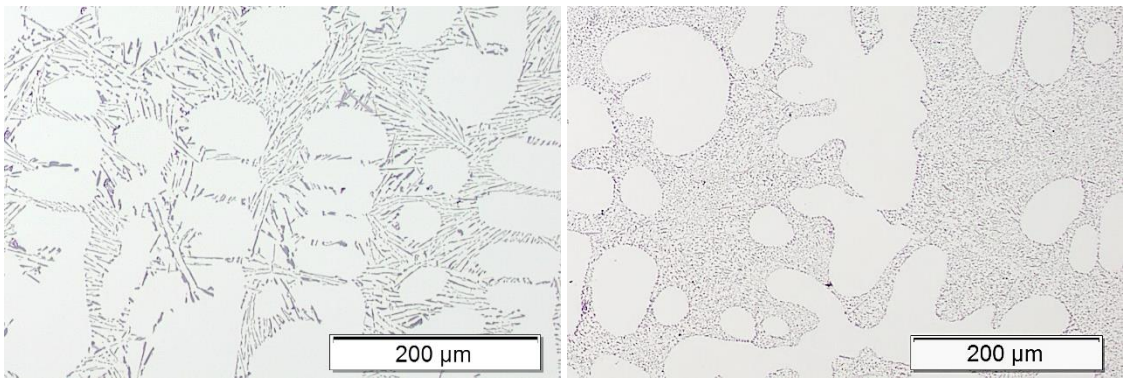

Figure 2. Morphology of a) unmodified eutectic Si and b) modified eutectic Si.

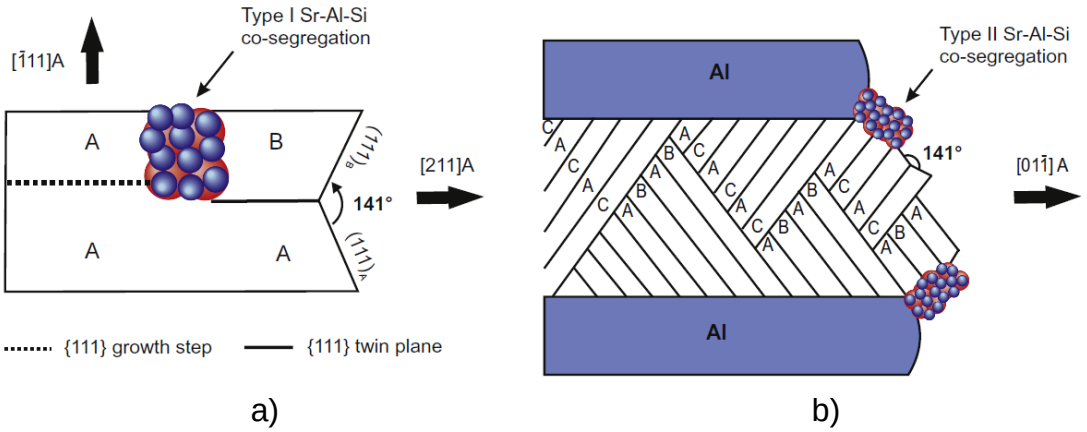

Figure 3. a) Impurity induced twinning mechanism and b) restricted TPRE growth [16]

Modifiers of significant industrial use are Na and Sr. Addition levels for Na are between 0.005 to 0.01 wt.% and Sr levels of 0.02 to 0.04 wt.%. Sodium dissolves readily in aluminium and is considered a more powerful modifier, but due to a very high vapour pressure, a large fraction boils off from the melt, and the resulting level is difficult to determine. Strontium on the other hand has a longer fading time as it will not evaporate at such high rate as Na, but oxidizes in contact with the atmosphere[17].

1.2.4 Grain refinement

While Si modification is related to the microstructural features being formed when the solidification of the eutectic takes place, grain refinement takes place at the beginning of solidification from the molten metal and pursues the formation of randomly oriented equiaxed grains. This is expected to improve feeding during casting, distribution of secondary phases, reduce the tendency to hot tearing and distribute porosity more evenly [18-20]. Grain refinement can be achieved via physical processes such as stirring or ultrasonication [21] or via inoculation with master alloys. Main grain refiner master alloys are Al-Ti, Al-Ti-B and Al-B [22]. The use of the different master alloys and the Ti/B ratio in the case of Al-Ti-B has been widely discussed related to the effectiveness of the inoculation [22, 23] and to the specific nucleant particles. These can be $TiAl_3$, TiB_2, TiC or AlB_2 [22].

Several models have been proposed to explain the grain refinement mechanism [22]. Easton & StJohn [20] classified them in two main groups: the nucleant paradigm and the solute paradigm. Those theories focused on the specific mechanism taking place during the heterogeneous nucleation where considered part of the former. The later included the theories focused on how the solute elements restrict the growth of grains once nucleation has already happened. They went on to suggest that for grain refinement to take place, both potent nucleant particles and segregation elements are needed [24]. This was later on formalized by StJohn et al. [25] in *the Interdependence theory* where nucleation occurs at the intersection of constitutional undercooling and the distribution of the potent particles in front of the interface according to eq.1.

$$d_{gs} = x_{cs} + x'_{dl} + x_{Sd} \qquad (1)$$

Where x_{cs} is the distance the already nucleated grain needs to grow to generate sufficient constitutional supercooling, x'_{dl} is the diffusion length from the solid-liquid

interface where the amount of constitutional supercooling (ΔT_{cs}) reaches its maximum value and x_{Sd} is the average interparticle spacing for the potent nucleants. x_{cs} and x'_{dl} together determine the nucleation-free zone where the constitutional supercooling is not enough to allow nucleation for the particle size considered. In a simplified version (Figure 4):

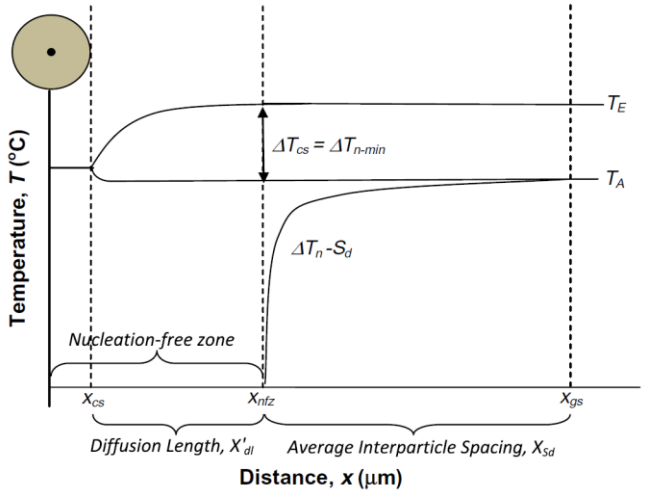

Figure 4. Simplification of the solidification pathway showing the three regions that determine the grain size: x_{cs}, x'_{dl} and x_{Sd}. The first two regions determine the zone were nucleation is not possible as proposed in the *Interdependence model* [25]

As occurred during modification, the grain refinement effect of inoculation has also been observed to fade [23], resulting in coarser grain sizes. One of the common mechanisms identified to produce fading is related to the settlement of the potent particles due to differences in density [26].Of special importance for Al-Si alloys is what has been termed as "Si poisoning", which seems to happen to some master alloys when the Si content exceeds 3 wt.% [21, 27-31] by formation of silicides [30, 32]. This poisoning effect with Si has not been observed for boron-rich master alloys, where improved grain refinement has been reported[33-36], but formation of SrB_6 compounds has been observed, binding the Sr and decreasing the efficiency of modification [19, 37, 38].

1.3 PROCESS VARIABLES

1.3.1 Melt Quality

The cleanliness of the melt will affect the soundness of the cast part. A lack of soundness in the cast part means foreign particles, oxide layers, defects such as pores or shrinkage and a corresponding loss of properties [39]. Sources of uncleanliness can be the ingots used for melting, refractory particles from furnace linings, oxides formed during melting, transport or inclusions from the recycling of alloys [40].

Besides that, due to a high solubility of hydrogen in liquid aluminium, melts are prone to absorb hydrogen. Sources can be the water vapour in the surrounding atmosphere, added fluxes, crucibles, combustion gases, refractories, foundry tools and even charge materials [12]. Liquid aluminium also oxidizes readily. In contact with the atmosphere it will form an oxide layer that slows down the hydrogen pickup. During the common handling of the melt, the protective oxide layer can fold over itself and entrap air to form what has been denominated bifilms [40]. Both the dissolved

hydrogen as well as the entrapped oxide films will have a detrimental effect in the cast component, as they have been identified to contribute to the formation and growth of defects such as shrinkage and gas porosities [12, 40]

Over the years, multiple techniques to characterize the quality of the melt have been proposed: Reduced Pressure Test (RPT), Fluidity tests, Porous Disc Filtration Apparatus (PoDFA), Pressure filtration (Prefil) or Laser Induced Breakdown Spectroscopy (LIBS) [41-43].

The RPT, as its name indicates consists of solidifying a melt sample under reduced pressure. The test was originally used as a mean to measure the dissolved hydrogen in the melt. Later on, determination of the density variation between the sample solidified under reduced pressure, compared to the atmospheric pressure sample allowed for the determination of the density index, with a low number indicating a lower tendency for pore formation. The working principle of the test is that, under such solidification conditions, bifilms will open up and unfurl, enabling their detection and leading to a reduction in density [40, 44]. An alternative use of the test was introduced by Dispinar and Campbell [45] as the sum of the maximum length of the pores in a cross section of a sample solidified under reduced pressure. Referred to as the bifilm index, a higher value would indicate a lower melt quality.

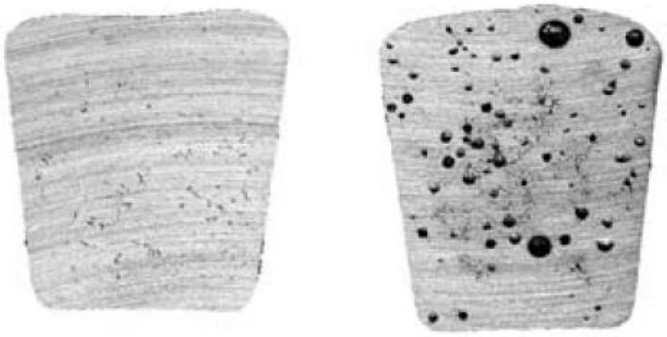

a) b)

Figure 5. Sectioned samples of a) atmospheric pressure and b) reduced pressure solidified melt samples [44].

Fluidity tests have also been proposed as a method to characterize the melt quality. Fluidity is determined as the distance the liquid metal traverses before stopping. The working assumption is that inclusions or oxide films will choke the flow of the melt and result in shorter fluidities [41, 44, 46]. The most accepted test method consists of pouring the melt into a spiral shaped mould (Figure 6).

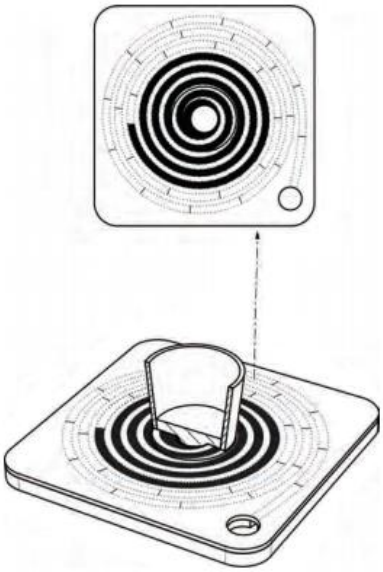

Figure 6. Spiral shaped fluidity test. Courtesy of Bryne AB

In the Prefil test (Figure 7) a crucible with melt is pre-heated and placed in a pressure chamber over a filter. The chamber is pressurised when the starting temperature is reached, forcing the material through the porous filter disk. Comparing the mass of melt that passes the filter to the time needed, a mass vs time curve can be plotted and the melt quality determined [47]. It has been discussed that the effectiveness of the technique is highly related to the filter used [48]. The complementary metallographic analysis of the "cake" formed over the filter is the basis for the PoDFA [49].

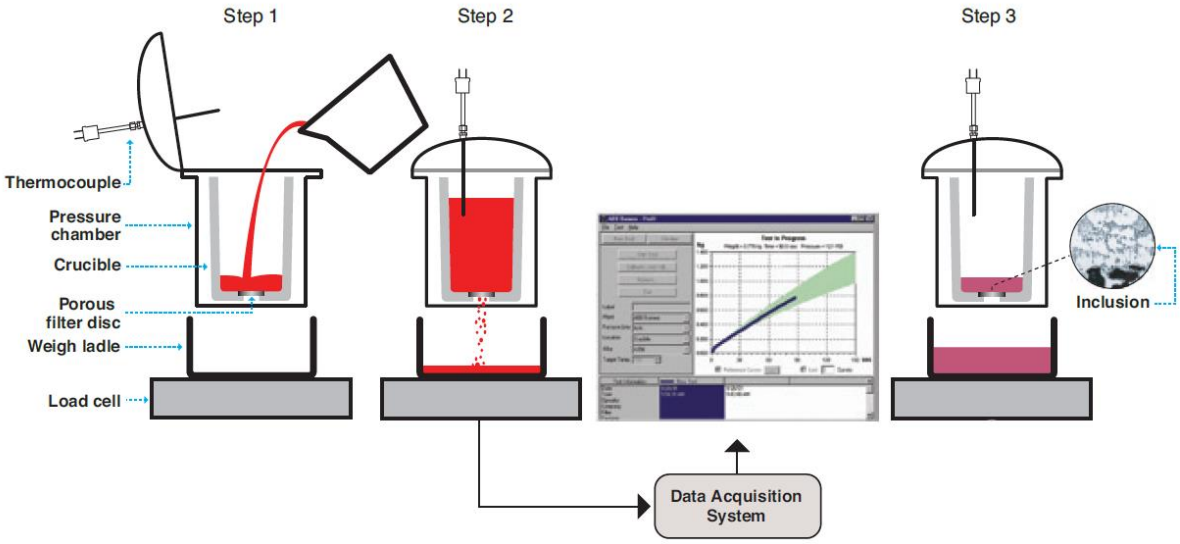

Figure 7. Schematic representation of the Prefil testing equipment [50].

1.3.2 Solidification

Solidification is the phase transformation from liquid to solid. The conditions under which solidification takes places will deeply influence the final microstructure thus influencing the properties of the cast component. Variables influencing the solidification include among others: chemical composition, modification, inoculation and cooling rate.

From a process point of view, the achievable cooling rates are one of the main variables. The rate at which heat can be extracted from the liquid will depend on the different mould materials coupled with how the melt is introduced in the mould. Cooling rates of 0.05-0.2 °C/s are common for plaster moulds or for dry sand while 50-500°C/s can be achieved in a metal die in HPDC [51]. Depending on the cooling rate, the coarseness of the microstructure will vary. With higher cooling rates, increasing undercooling takes places and features such as dendrite size, particle size and shape are refined and become smaller [52].

The local solidification time can be correlated to the secondary dendrite arm spacing (SDAS) through the empirical relation in eq.2:

$$SDAS = Kt_f^n \qquad (2)$$

Where t_f is the solidification time, n and K are alloy specific constants [53] and SDAS is determined as shown in Figure 8.

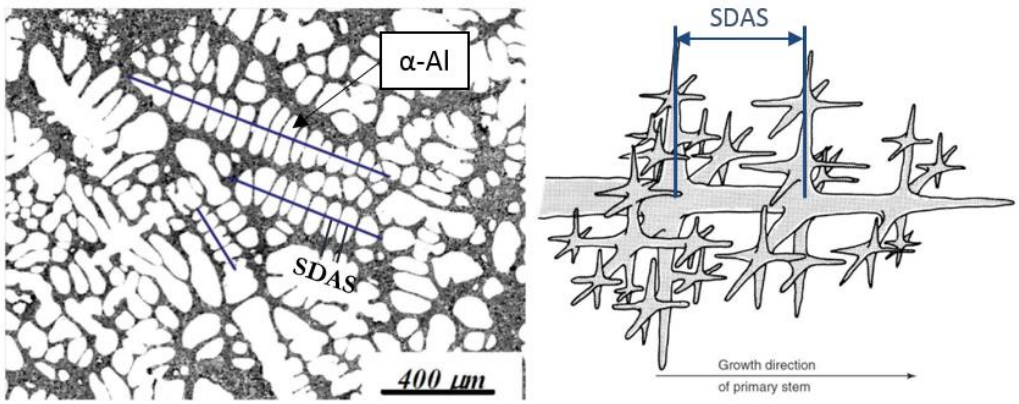

a) b)

Figure 8. Secondary dendrite arm spacing a) Line intercept method [54] and b) three dimensional representation [55].

1.4 POST-SOLIDIFICATION VARIABLES

1.4.1 Heat treatment

The most relevant post-solidification treatment to further tailor the performance of Al-Si alloys alloyed with Cu and/or Mg is a proper heat treatment. The aim of the heat treatment is to control the precipitation size and fraction of nano-sized intermetallics within the Al matrix. Doing so, the microstructure of the cast component can be further modified to achieve set-up demands upon strength and/or ductility. Different intermetallic phases need different time and temperatures to dissolve and homogenize depending on system and process variables [56]. Due to this, the specific heat treatment applied to a gravity cast component will be different than that applied to a HPDC component.

The different heat treatment solutions are generally a combination of the following three stages [5]:

1. Solution treatment at temperatures close to the eutectic temperature of the alloy to dissolve soluble phases (generally Mg- or Cu- rich), homogenize alloying elements and to spheroidize eutectic Si particles.

2. Quenching, which consists on a rapid cooling of the component, generally to room temperature, and is aimed at obtaining a supersaturated solid solution of solute atoms and vacancies within the Al matrix.
3. Age hardening, either at room temperature (natural ageing) or at elevated temperature (artificial ageing) to cause precipitation from solid solution.

When these three stages are carried out to achieve a peak aged condition, the treatment is referred to as T6 treatment. Due to the solution treatment stage giving rise to blisters in the surface of cast parts, it is not generally applied to HPDC components. A T5 treatment, consisting of a controlled cooling after solidification with an artificial ageing is applied instead [57].

1.5 KNOWLEDGE GAPS

The existing knowledge, observed in the literature, provides information on how the properties of the cast component can be controlled. However, contradictory information has been observed and several gaps remain in our understanding.

Although the key variables effecting the resulting component are known [1], noticeable variation of properties in cast aluminium components is still observed and the interrelations between them are not fully investigated and understood. Additionally, as previously discussed, the melt quality and the tools to measure it have been widely studied. The effectiveness of these techniques has in general been studied separately from the effects of melt quality on the component properties [46, 47, 58]. In addition, results are generally difficult to compare as the working principles of the techniques are different and producing specific levels of melt quality is problematic, due to all the different features that can influence it.

Regarding modification and grain refinement treatments, contradictory results have been observed in relation to the efficiency of treatment, poisoning and fading effects and with respect to the effect they have on mechanical properties. Some authors have shown that grain refiner additions improve mechanical properties [59, 60], others reported otherwise[38, 61]. The differences observed could be related to different holding times and cooling rates.

If we are to produce high performing cast aluminium alloys, such contradictions need to be clarified and the gaps need to be filled.

CHAPTER 2

RESEARCH APPROACH

CHAPTER INTRODUCTION

In this chapter, the purpose and aim of the thesis are described, followed by a description of research activities and research methods.

2.1 PURPOSE AND AIM

The aim is to understand and clarify how the different variables during the process of component casting (melt quality, solidification process and the alloy selection) affect the material structure (microstructure, macrostructure and defects) that governs the mechanical properties. This will provide the base for control and assurance of cast component performance in terms of minimized variations in properties.

2.2 RESEARCH DESIGN

2.2.1 Research perspective

Materials science as an interdisciplinary field based on chemistry, physics and engineering inherits the empirical approach from the natural sciences. By using deductive reasoning, the objective is to obtain specific conclusions from general principles or premises through hypothesis testing to validate said conclusion [62].

First, the topic of interest is defined by taking into account the industrial and societal needs. Based on the topic of interest, an information gathering process is followed to increase the knowledge in the field, identify contradictions, relevant variables and set the limitations, leading to the definition of a hypothesis. Experiments to validate or refute the hypothesis are designed and performed and through data collection and analysis a general law can be stated.

The iterative process of information gathering involved retrieval, selection and evaluation of relevant information. The main information resources were online databases such as Scopus and Web of Science, granting access to various publications.

2.2.2 Research questions

The reviewed literature raised certain questions regarding the different variables involved in the process of component casting. In some cases, conflicting results were observed.

The current research therefore aims at understanding the relationships between the main variables in the casting process. More specifically, this work aims to clarify and connect the melt treatment, the solidification process and the alloy selection to the

material structure (microstructure, macrostructure and defects) and hence to the mechanical properties. It can be phrased in the following research questions:

1. How can we, by appropriate selection of system, process and post-process variables, produce high integrity castings?

The reviewed literature reported the key sets of variables that need to be controlled. The possibility to influence them and use them to our advantage is explored in this study.

2. How can Al-Si melt quality be reliably characterized?

A reliable way of assessing the level of undesirable inclusions in the melt is needed in order to ensure that the processes downstream receive the optimal material. The damage mechanisms associated with such inclusions needs to be characterized.

3. How are microstructure and mechanical properties correlated to additions of grain refiner and Si modifier coupled with the casting process?

Previous studies have reported contradictory results on both structure and mechanical properties. The interrelations need to be clarified for adequate system variables and process variables selection.

2.2.3 Research strategy

As has been introduced, the key sets of variables are interrelated. To produce relevant knowledge, isolation of the different effects is intended. This is achieved by holding all other variables constant except the variable of interest (*caeteris paribus* assumption). In that sense, the work can be grouped under three main topics:

- State of the art application; Supplement I is focused on achieving certain tensile and fatigue properties by means of selecting an appropriate trio of system, process and post-process variables according to the state of the art found in the literature. Process variables contemplated the use of sand and plaster casting; system variables consisted on the use of two different alloys: EN AC-42100 and EN AC-42100 with an addition of Cu. The post-solidification variables, as-cast and heat treated, were fixed in one system variable (one alloy) but depended on the solidification process. The options distribution is presented in Figure 9.

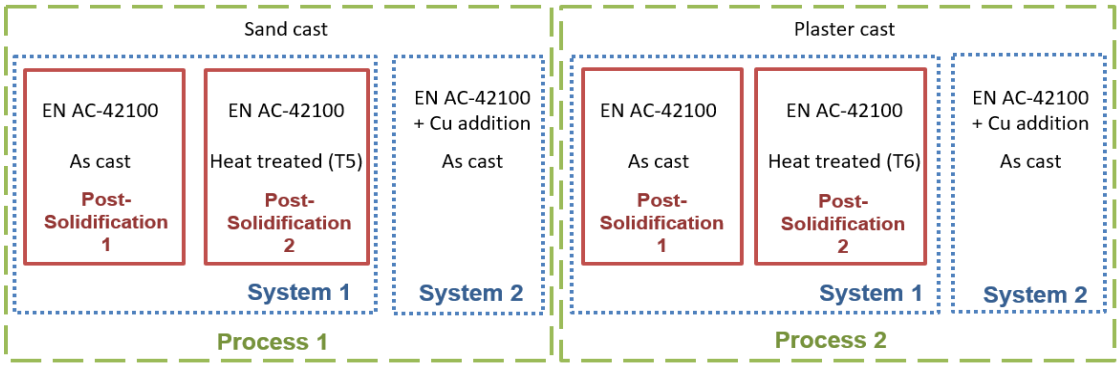

Figure 9. System, process and post-solidification variable distribution.

- Study of the main effects of melt quality; SupplementII consists on the application of different melt quality measurement tools to a fixed alloy

composition and a controlled tilt casting process. Through the tilting method, effects of system variables and defects from the casting process are avoided.

- Effect of grain refinement and modification; treated in Supplements III and IV, studies the connection between system variables, such as grain refinement and modification, to process variables regarding the solidification rate. Clarification of the effect of the resulting microstructural features is sought. A clean melt is produced from pure metals and subsequently directionally solidified.

Relationships between the three topics are stablished by means of comparable microstructures and by the characterization of resulting mechanical properties under the assumption that their effects are additive.

2.3 MATERIALS AND EXPERIMENTAL PROCEDURE

2.3.1 Alloys

The experimental work in this thesis complied 3 main alloys; two were commercially available alloys (EN AC-42100 and EN AC-46000) and the other was an Al-10Si alloy prepared from pure Al and Si. Standard composition (SS-EN 1706:2010) for the commercial alloys and intended composition for the Al-10Si alloy are outlined in Table 1.

Table 1. Standard and intended composition for the alloys used in wt.%

Alloy	Si	Fe	Cu	Mg	Ti	Al
EN AC-42100	6.5 to 7.5	0.15	0.03	0.30 to 0.45	0.18	Bal.
EN AC-46000	8.0 to 11.0	0.6 to 1.1	2.0 to 4.0	0.15 to 0.55	0,20	Bal.
Al-10Si	10	0.10	0	0	0	Bal.

The EN AC-42100 alloy (Al-7Si-0.3Mg) was cast in sand and plaster moulds in both its standard composition and alloyed with 1.7-2 wt.% Cu.

The EN AC-46000 (Al-9Si-3Cu(Fe)) alloy was used for melt quality measurements. The quality was degraded by adding 25 and 50 wt.% machining chips when melting. Conditions are name correspondingly to the addition level; L00, L25 and L50 for reference melt, 25 wt.% addition and 50 wt.%.

The Al-10Si was used as the representative alloy for common commercial alloys. Conditions with Si modifier addition (+Sr), grain refiner addition (+GR) and both (+Sr+GR) were produced, besides the base alloy for directional solidification. The alloys contained no other alloying elements to evaluate the sole effect of grain size and Si modification.

2.3.2 Casting

2.3.2.1 Sand mould

Melting of the EN AC-42100 alloy was carried out in a 100 kg furnace. For Cu alloyed condition, Cu chips wrapped in Al foil were pushed to the bottom of the crucible.

Degassing was accomplished by adding tablets prior to addition of grain refiner and Na for modification. The melt was then held at 720°C. Bending fatigue geometry samples were cast by pouring from a ladle into the five-sample, two-part mould.

2.3.2.2 Plaster mould

The melting and Cu addition was carried out in the same way as for the sand casting process. In this case, grain refiner and Al-10Sr for modification additions and degassing with N_2 for four and a half minutes was performed the night before casting. Two samples per mould, also in the bending fatigue geometry were cast in two-part moulds preheated to 200°C.

2.3.2.3 Tilting tensile mould

Commercial EN AC-46000 ingots were melted in a 50 Kg resistance furnace. The machining chips were added as compressed pucks in the bottom of the crucible before melting. Chemical composition of L00 and L25 was corrected with suitable master alloys to match the measured values for the L50 condition. The melt was only stirred when additions were made to ensure proper dissolution. The melt was then held at 765°C.

For casting, the melt was poured into the feeder section of the steel tilting mould with a ladle. The mould was previously coated with graphite and preheated to 250°C

2.3.2.4 Directional solidification

The Al-10Si melt was prepared with pure Al and Si in a 6-kg resistance furnace. Additions of grain refiner and/or modifier were done with Al-5Ti-1B and Al-10Sr master alloys in rod shape, wrapped in Al-foil and preheated to 200°C to remove possible moisture. The melt was held at 730°C. After 30 min of homogenization, cylindrical bars were cast in a graphite coated Cu mould preheated to 250°C. Oxide cleaning and stirring without breaking the oxide surface was performed prior to casting to avoid entrapment of oxides and settlement of particles.

The cast bars were remelted under Ar atmosphere at 730°C for 30 minutes in a vertical furnace in graphite coated steel tubes. By withdrawing the tubes from the furnace at different rates with different cooling media, a controlled, directional solidification was achieved. Three different rates were used: 3 mm. s^{-1} (water cooled), 0.3 mm. s^{-1} (water cooled) and 0.03 mm. s^{-1}(air cooled).

2.3.3 Heat treatment

2.3.3.1 T5 Heat treatment

Samples cast in sand moulds received a T5 treatment at 180°C for 5 hours.

2.3.3.2 T6 Heat treatment

Plaster cast samples received a T6 treatment consisting of solution heat treatment at 530°C for 6 hours (in a Nabertherm L40/11 furnace), quenching in hot water, natural ageing for 24 hours and an artificial ageing at 180°C for 5 hours (in a Nabertherm TR-120 furnace with air circulation).

2.4 CHARACTERISATION

2.4.1 Melt

The characterization of the melt quality (suppl. II) involved the following techniques:

2.4.1.1 Reduced Pressure Test

The reduced pressure test (RPT) consisted on solidification, under reduced (80 mbar) and atmospheric pressure, of 80 g melt samples scooped with boron nitrate coated stainless steel cups. Samples were taken at 5 different occasions from each melt. The density of both atmospheric and reduced pressure samples was measured using the Archimedes' principle. The density index (DI) was calculated following eq.3.

$$DI = \frac{\rho_{atm} - \rho_{RPT}}{\rho_{atm}} \times 100 \qquad (3)$$

Where ρ_{atm} and ρ_{RPT} are the density of the samples solidified at atmospheric and reduced pressure respectively.

2.4.1.2 Hydrogen content

Hydrogen content measurement was performed when a RPT was conducted by using the Alspek H equipment.

2.4.1.3 Fluidity

Fluidity of the different alloy conditions was measured by spiral fluidity tests. The feeding cup for the test was first filled with melt with a ladle. Once the temperature in the feeding cup reached 720°C, the melt was allowed to flow. Fluidity values were determined from the distance traversed within the mould. Measurements were performed 5 times per melt.

2.4.1.4 Prefil

Three Prefil measurements were performed for each melt. 2 kg of melt were sampled by casting in 70 mm diameter steel cylindrical moulds. The top part was then cut to produce 1.4 kg samples that were remelted in an induction furnace and poured in the Prefil equipment. The variation of filter permeability was compensated with an online model and a melt cleanliness (MC) number was calculated based on the build-up of cake inclusions on the filter.

2.4.2 Chemical composition

Chemical composition analysis was measured by Optical Emission Spectroscopy using a Spectromaxx LMX06. For all melts, chemical analysis samples were cast in a steel mould for fast solidification and cooled with water.

The composition along the directional solidified samples was measured in nine locations along the axis in order to monitor possible changes in composition after the remelting procedure (suppl. III).

2.4.3 Sample preparation

2.4.3.1 Tensile testing specimens

Samples for conventional tensile testing were machined in both flat (Supplement I) and round geometries (Supplements II, III and IV). The corresponding geometries can be found in Figure 10.

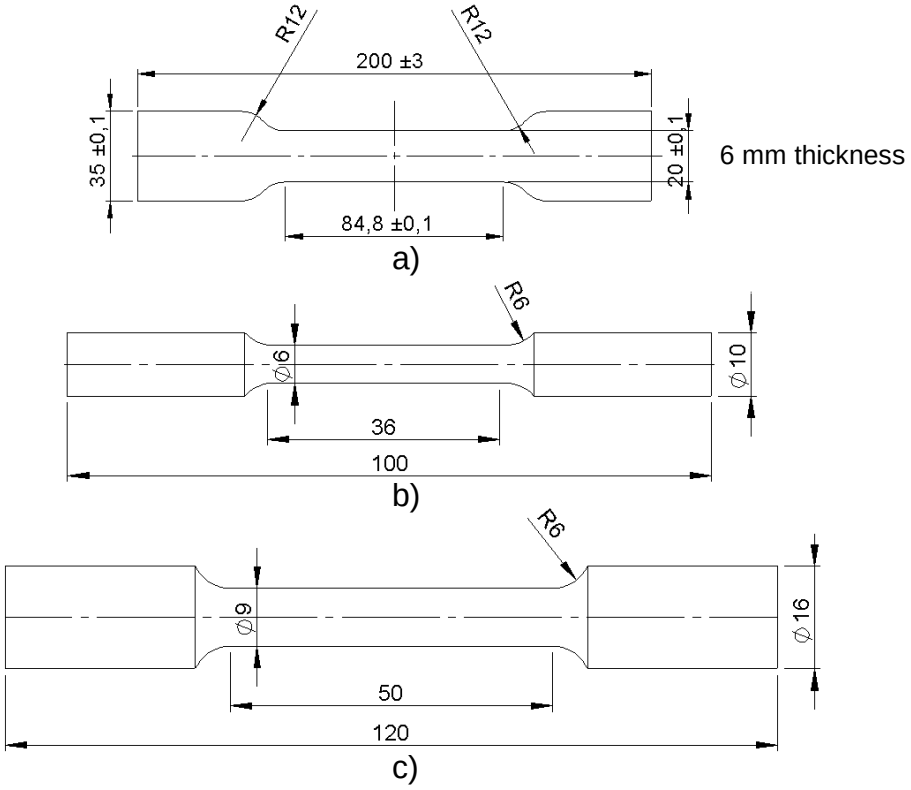

Figure 10. Tensile test geometries for the a) flat and b-c) round samples used in this work (dimensions in mm).

Flat, down-sized samples for in-situ tensile testing Figure 11 were prepared by machining, followed by polishing using standard practices. A notch in the middle of the gauge length was made to ensure cracking in the field of view.

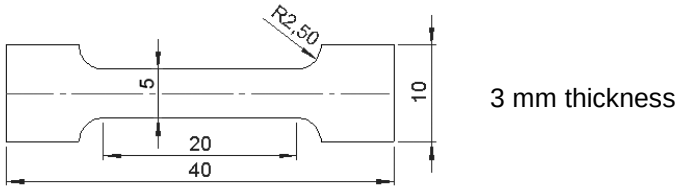

Figure 11. In-situ tensile test geometry (dimensions in mm)

2.4.3.2 Microstructure analysis specimens

Samples from the various tests were selected, cut, hot mounted, ground and polished for microstructural characterization; RPT were cut in half, along their symmetry axis (Figure 12a). From fluidity tests, the top of the feeder, the gate and the tip were extracted (Figure 12b). From representative tensile test samples, fracture areas were selected for optical microscopy. Cross and longitudinal sections from the area corresponding to the gauge length of directional solidified samples were also

prepared from all conditions. Samples for grain size measurement were etched with a 10% $CuCl_2$ solution for 15 sec.

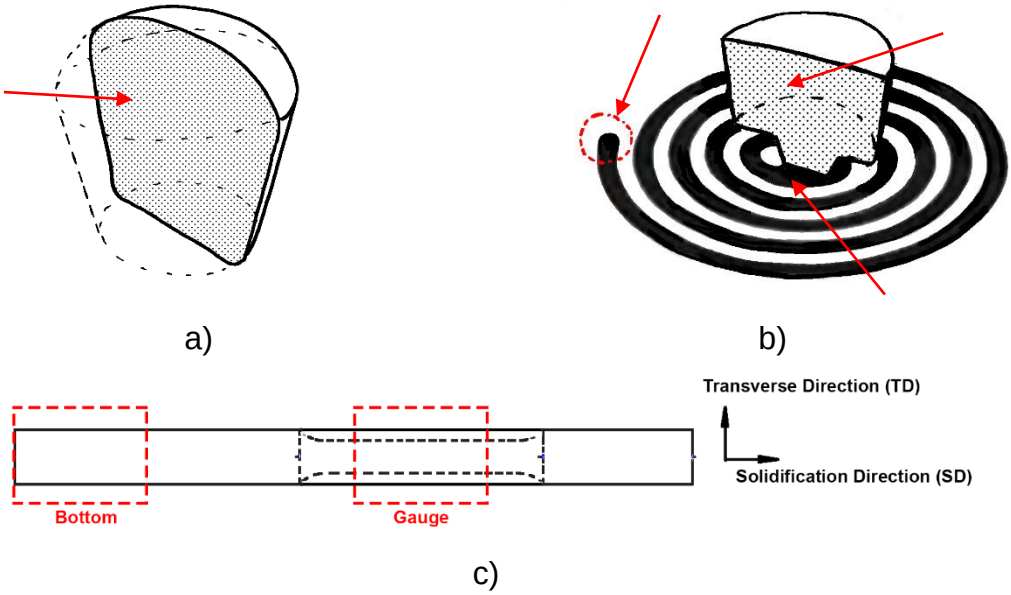

Figure 12. Schematic representation of areas selected for microstructure analysis in a) RPT b) fluidity tests and c) directional solidified samples.

2.4.4 Mechanical properties

2.4.4.1 Tensile testing

Conventional tensile testing was carried on with a Zwick/Roell Z100 equipped with a 100 kN load cell. The results from the melt quality samples were fitted to 2-parameter Weibull distributions by the maximum likelihood method according to the guidelines provided by Tiriakioglu and Hudak [63].

In-situ tensile test was performed with a Kammrath & Weiss stage inside a TESCAN LYRA3 SEM equipped with an electron back scattered diffraction (EBSD) detector.

2.4.4.2 Fatigue testing

Bending fatigue tests were conducted at a stress rate of R=-1 (fully reversed load) and 12 Hz frequency. Samples not failing after 3 x 10^6 cycles were considered run outs. The results were fitted to a 3rd grade semi-logarithmic S-N curve by the maximum likelihood method.

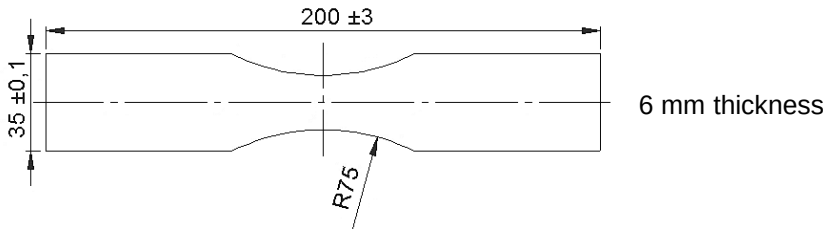

Figure 13. Bending fatigue test geometry (dimensions in mm)

2.4.5 Microstructure analysis

2.4.5.1 Optical microscopy

Microstructures were studied by optical microscopy with an OlympusGX71F. Secondary dendrite arm spacing (SDAS) was measured by the linear intercept method. For the directional solidified samples (suppl. III & IV), grain size was determined from both the etched longitudinal and cross section metallographic samples and from EBSD maps using the linear intercept method as described in ASTM E112-96. In the case of long columnar grains, the column width was reported.

Image analysis was performed with the Olympus Stream Motion Desktop 1. 9. 1. Bifilm quantity was determined according to eq. 4 from 600 dpi scans of the cross section of RPT. Detection limit was set to porosities with an area equivalent to a 0.2 mm diameter circle.

$$Bifilm\ Quantity = \frac{BI}{area} = \frac{\sum(pore\ length)}{total\ area} \qquad (4)$$

Porosity in the tip of the fluidity test spirals was characterized over a total area of at least 250 mm^2.

2.4.5.2 Scanning Electron Microscopy (SEM)

Fracture analysis of tensile tested samples was performed on a TESCAN LYRA3 SEM for samples selected as representative of the different melt qualities (suppl. II). For each melt quality, the area fraction of defects was determined from binary images as the quotient of defect area and total area regardless of the defect type. According to the quality index, the best, average and worst performer were picked. Selection of defects for the binary images was carried on with a Wacom Cintiq interactive pen display.

2.4.5.3 Energy Dispersive X-ray Spectrometry (EDS)

Qualitative composition maps of Al, Si, Sr, Ti and B were determined from the bottom of directional solidified samples by EDS in a JEOL 7001F SEM to determine possible settlement of particles.

2.4.5.4 Electron Backscattered Diffraction (EBSD)

Depending on expected grain sizes, areas up to 2.5 x 4.0 mm^2 in both longitudinal and cross section samples were characterized using an EDAX detector mounted on a JEOL 7001F SEM. The acceleration voltage of 20 kV and step sizes ranging between 1.9-4 µm were used for that purpose. All EBSD maps were further analysed using TSL-OIM software with coefficient index (CI) standardization and exclusion of points with CI less than 0.1.

CHAPTER 3

SUMMARY OF RESULTS AND DISCUSSION

CHAPTER INTRODUCTION

In this chapter, the main results of the appended papers are summarised and discussed. This chapter is divided into three parts according to the proposed research strategy: state of the art, melt quality evaluation and grain refinement and modification.

3.1 STATE OF THE ART

The concept of performance assurance by controlling the three key sets of variables (system, process and post-process) was tested according to the scientific and industrial state of the art practices. This is treated in Supplement I. The characterization of the resulting microstructures is presented first, followed by the effect on the mechanical properties.

3.1.1 Microstructure characterization

The two processes chosen (sand and plaster mould casting) were characterized through the resulting SDAS, as it is related to the local cooling rate. A SDAS value of 22 ± 3 μm was determined for samples cast in sand moulds and 53 ± 7 μm was determined for plaster cast samples. The two processes are referred to from now on as SDAS 20 and SDAS 50 for simplicity. It deserves mentioning that Cu additions, while not statistically significant, slightly decreased the SDAS to 20 ± 3 μm and 47 ± 6 μm respectively.

Eutectic Si modifier was added for both processes. Nevertheless, analysis of the resulting microstructures (Figure 14) revealed different degrees of modification for the SDAS 20 and SDAS 50 processes. While SDAS 20 samples displayed a well modified fibrous eutectic Si morphology, those for the SDAS 50 presented a mixed structure, with areas of well modified eutectic Si and areas of flake-like Si particles. According to the chemical analysis, the level of modifier in SDAS 50 samples should have been enough to achieve a fully modified eutectic Si morphology. As the chemical analysis can only detect the amount of the element being measured (in this case Sr), while the level is adequate, it is possible that it is not in free form and hence cannot take part in the modification mechanism.

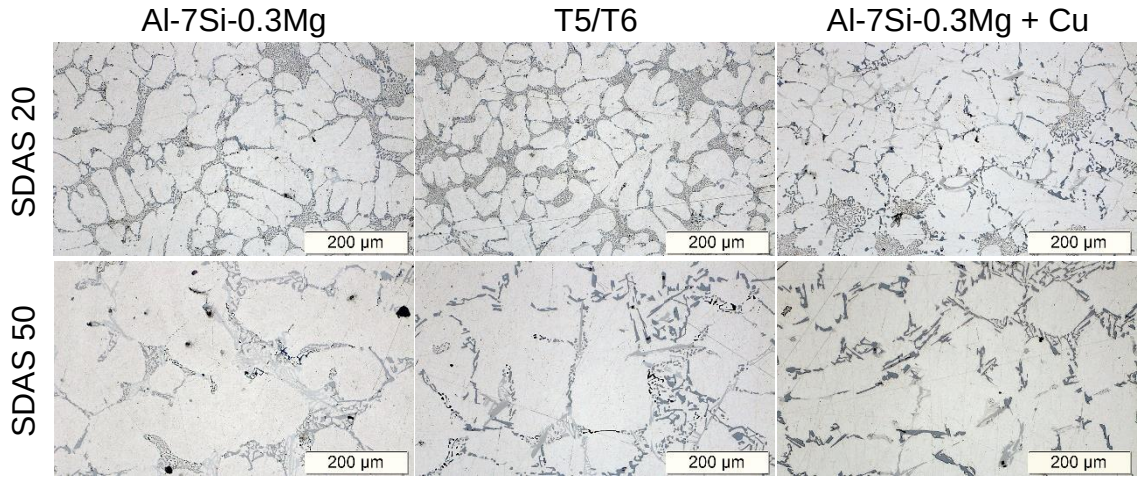

Figure 14. Representative microstructures for the different combination of system, process and post-process tested. (a-c) Sand casting (SDAS 20) and (d-e) Plaster casting (SDAS 50)

3.1.2 Effect on mechanical properties

3.1.2.1 Tensile properties

The mechanical properties achieved by variation of process (sand/plaster), system (Al-7Si-0.3Mg/ Al-7Si-0.3Mg+Cu) and post-process (T5/T6 respectively) are presented in Figure 15. If the Al-7Si-0.3Mg in as-cast state is used as reference, both heat treatment and Cu addition resulted in increased yield strength (YS) with a decrease in % elongation regardless of the process. The T5 treatment, applied to the SDAS 20 samples produced an increase in ultimate tensile strength (UTS) of 11% while the T6 treatment applied to the SDAS 50 samples resulted in a 92% increase.

The performance control values were set to achieve properties similar to the minimum values for die casting EN AC-46000 as stated in the SS-EN 1706:2010 standard (UTS=240 MPa, YS=140 MPa and elongation<1%). Only the SDAS 50 T6 treated samples reached UTS values comparable, but the corresponding YS was too high and the elongation values were too low. In terms of YS, the T5 and Cu addition sand cast (SDAS 20) samples exhibited adequate values but only the T5 treated condition resulted in the correct elongation values.

Comparing the Al-7Si-0.3Mg as-cast values, with the same elongation to fracture, the sand casting process (SDAS 20), with values above those of SS-EN 1706:2010 standard, resulted in higher UTS and YS values than the plaster casting process (SDAS 50). This was due to a finer microstructure, with smaller intermetallic phases and a higher degree of Si modification. The finer microstructural features justified the selection of a T5 treatment for the SDAS 20 samples while a T6 would be needed for the SDAS 50, as a higher level of solid solution was expected in the as-cast state. The tensile results observed for the T6 treated condition showed that while UTS values were acceptable, YS became too high in peak aged condition, and a too high loss in elongation was experienced. According to the literature, considering the microstructure coarseness, an underaged T6 treatment could result in a smaller loss of elongation and lower YS.

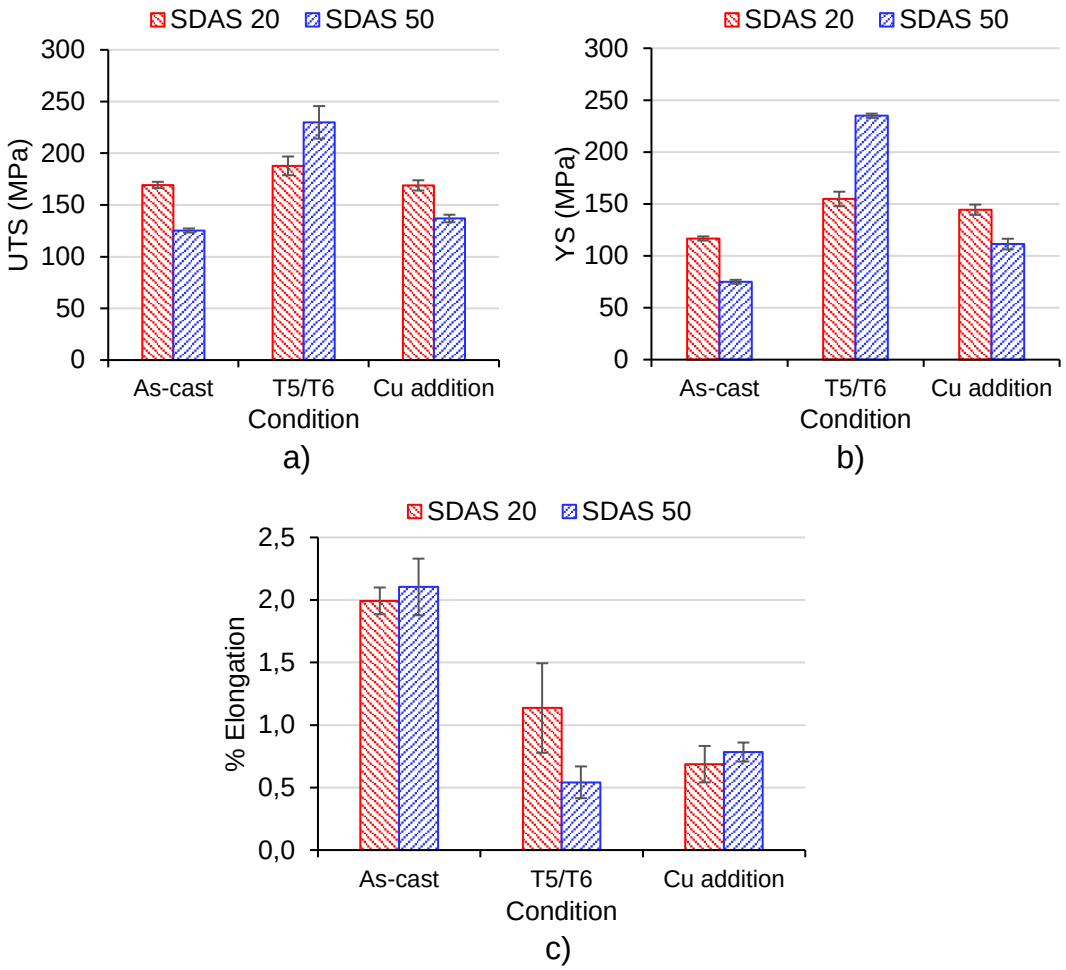

Figure 15. a) UTS, b) YS and c) %elongation for the two processes (SDAS 20 and SDAS 50) in the as-cast, heat treated and Cu addition conditions.

3.1.2.2 Fatigue properties

Regarding the fatigue properties, as can be observed in Figure 16, the sand cast samples (SDAS 20) performed similarly, regardless of the T5 treatment or the Cu addition. This could be due to the microstructural features such as intermetallics and Si shape and morphology being in the same size range for the three conditions. A similar conclusion could be drawn for the reference Al-7Si-0.3Mg alloy in as-cast condition and the Cu addition for the plaster cast samples (SDAS 50). These two conditions were also found to perform similarly. The T6 treated condition on the other hand exhibited an increase in fatigue resistance values. The solid solution strengthening of the α-Al matrix through the heat treatment was probably the cause for such improvements. When qualitatively considering the sample surface, plaster casting exhibited less roughness overall. Even so, the fatigue performance was higher for the sand cast samples, implying that in this case, roughness played a secondary role compared to internal near surface characteristics such as possible pores, precipitates, inclusion or secondary phases played

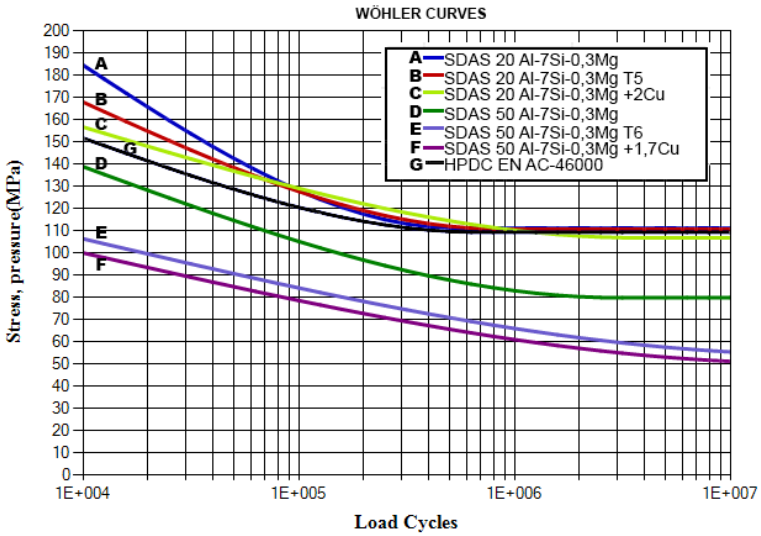

Figure 16. Wöhler curves for the two processes (SDAS 20 and SDAS 50) in the as-cast, heat treated and Cu addition conditions

3.2 MELT QUALITY

Assessment of commonly used techniques to measure melt quality (treated in Suppl. II) was approached for the first time in connection to the effect that these different melt qualities would have on tensile properties. Three different melt qualities were prepared: clean (L00), 25 wt.% (L25) and 50 wt.% (L50) machining chips additions. The alloy composition was corrected to ensure no change in the alloy system. Hydrogen content, RPT, fluidity, Prefil and tensile tests were performed. The characterization of the melt is presented first, followed by the effect the melt qualities have on the tensile properties.

3.2.1 Melt quality characterization

The hydrogen content was observed to be the same for quality levels L00 and L25 and to decrease for the L50 casting. The measured humidity levels next to the furnace were 39, 35 and 48% for L00, L25 and L50 respectively. The measured values can be found in Figure 17a. The results from the RPT (Figure 17b) were found to be inconclusive; density index (DI) did not significantly change and only the L25 quality exhibited an increase in scatter. The bifilm index (BI) also did not show a significant increase, but the scatter increased when machining chips were added.

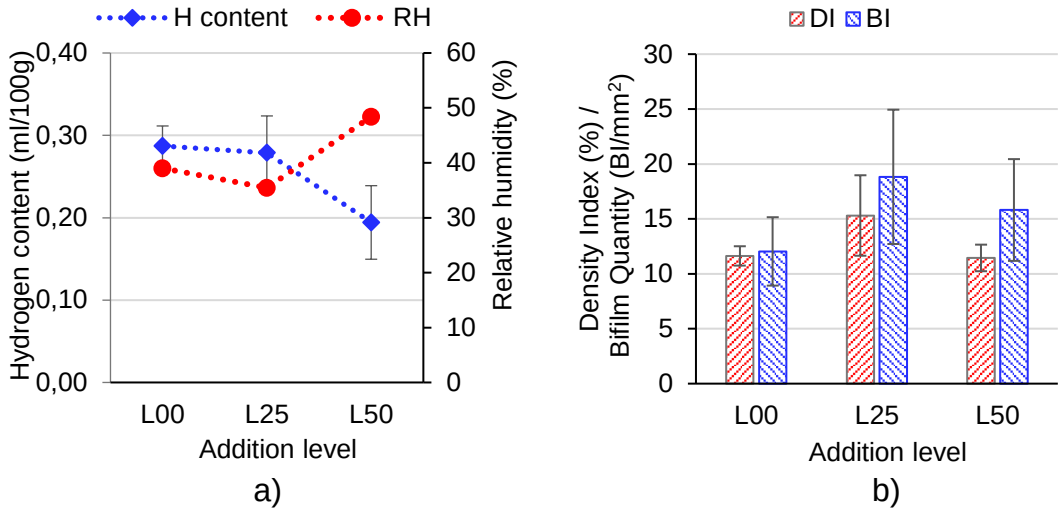

Figure 17. a) Hydrogen content and relative humidity levels and b) Density Index (DI) and Bifilm Quantity for the three melt quality levels tested.

Higher relative humidity would generally result in a faster absorption of hydrogen by the melt. As chemical composition correction was needed for both L00 and L25 melts, the lower hydrogen content observed for the L50 melt could be due to shorter contact time for hydrogen pick-up.

Fluidity and Prefil measurements did not show significant variation either (Figure 18a). Fluidity did not decrease with the machining chips addition and the scatter only increased for the L25. The melt cleanliness number increased with additions but within the values considered to correspond to "moderately clean" melts [64]. The corresponding mass-time curves (Figure 18b) further confirmed these results, with L25 and L50 overlapping.

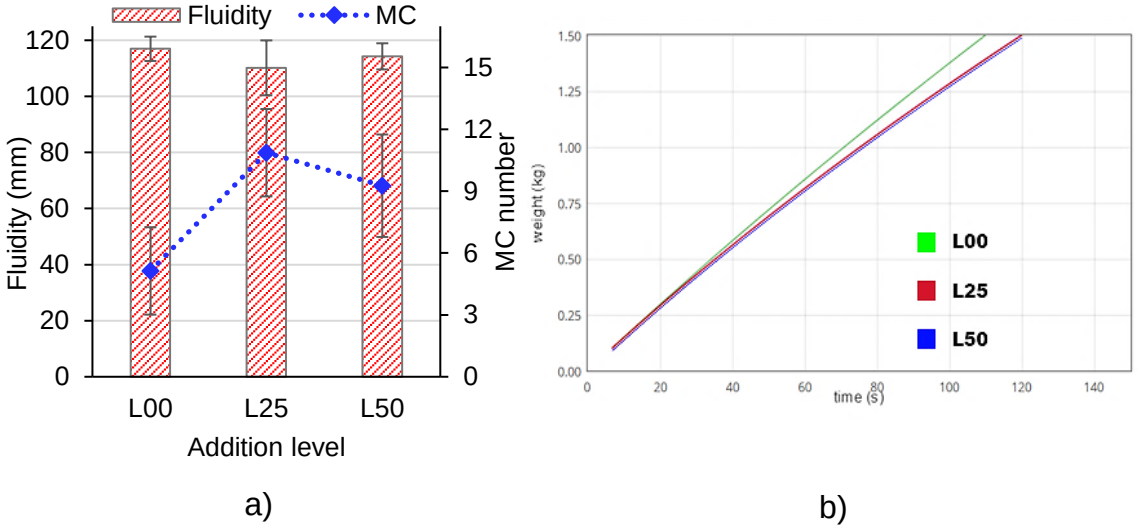

Figure 18. a) Fluidity and melt cleanliness number and b) Prefil mass-time compensated curves for the three melt quality levels tested. L25 and L50 mass-time curves overlap.

The microstructural analysis of RPT and fluidity tests revealed a layer of folded oxides towards the top of the samples (Figure 19b, c and Figure 20a). In RPT samples, these oxides were only found above a marked band of big round porosity in L25 and L50 quality levels. Below these bands, the appearance of the defects was that of

shrinkage porosity. The samples solidified at atmospheric pressure also presented accumulation of folded oxides on the top, but no big pores were found in the boundary between the oxides and the rest of the sample.

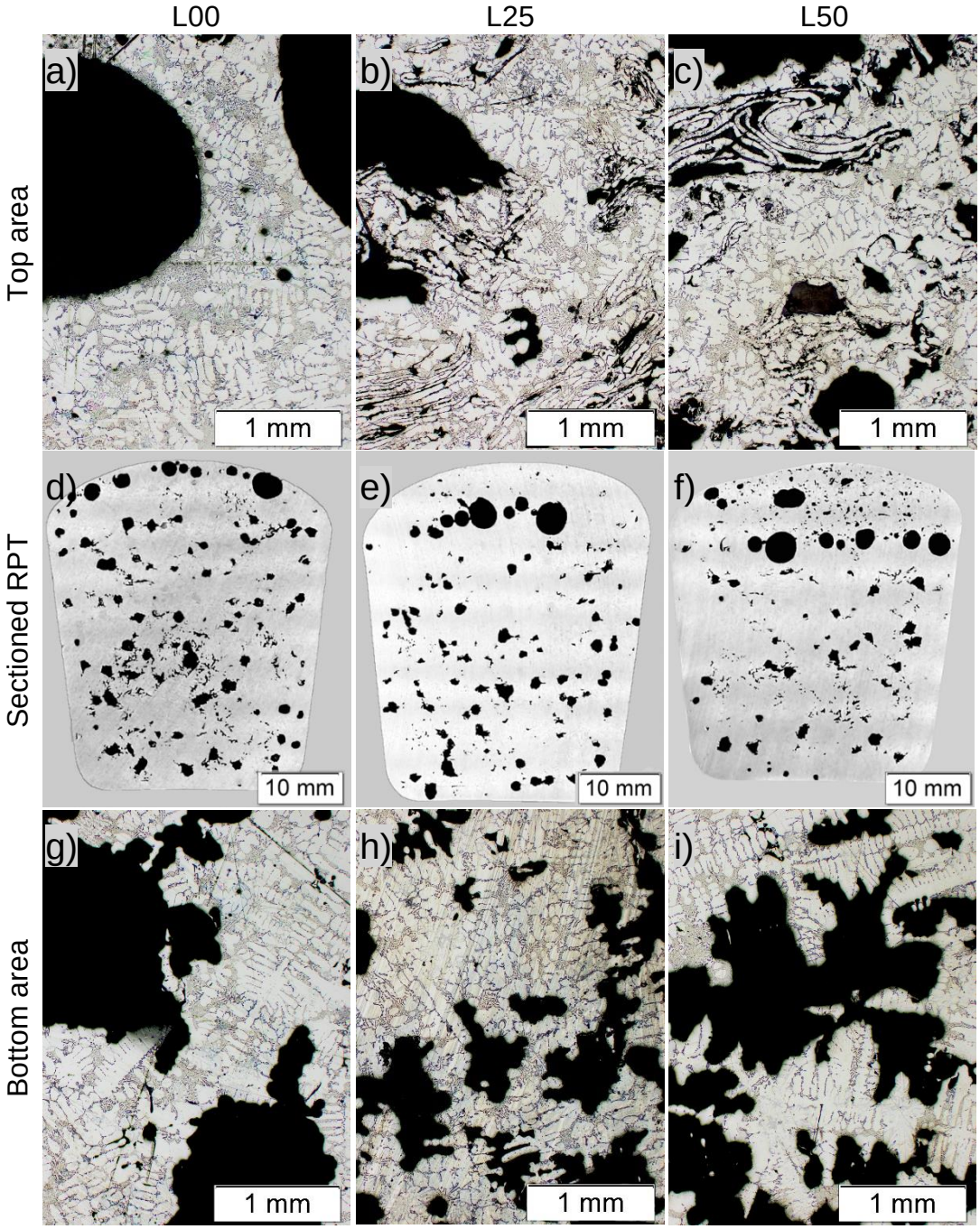

Figure 19. Typical RPT microstructures of top area (a-c), sectioned samples (d-f) and (g-i) for L00, L25 and L50 melt qualities respectively.

The fluidity tests presented these folded oxides in the top of the feeder. The tip of the spirals revealed rounded gas porosity of various sizes. The characterization of these sections by image analysis (Table 2) revealed a decrease in pore area fraction and in pore size with machining chip addition. On the other hand, the number of pores increased.

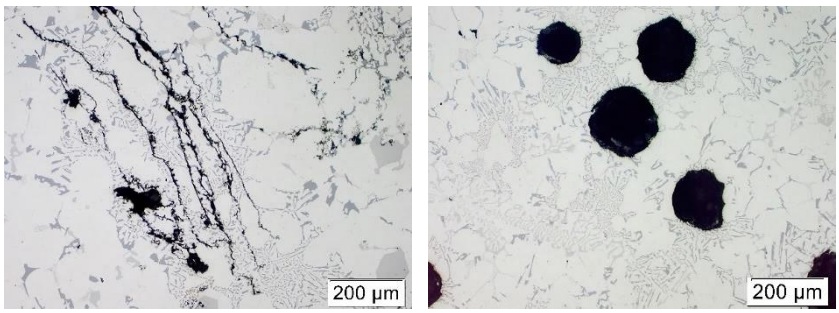

a) b)

Figure 20. a) Oxide film in top of fluidity test and b) rounded gas pores in the tip of fluidity test for the L50 melt quality.

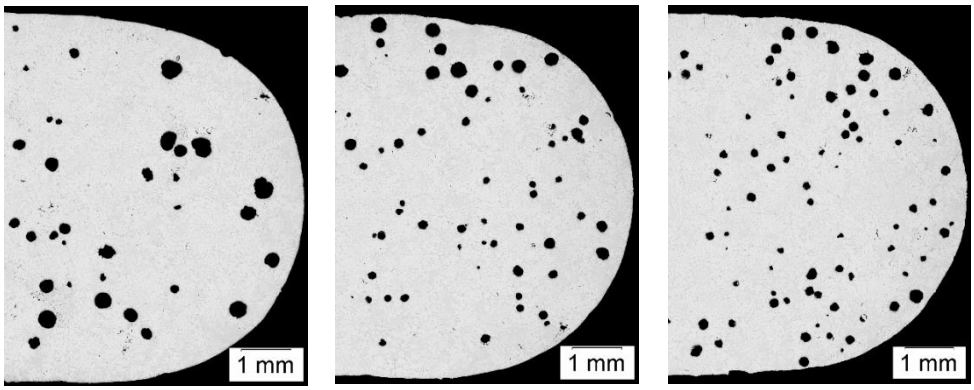

a) L00 b) L25 c) L50

Figure 21. Tip of fluidity test for a) L00, b) L25 and c) L50 melt qualities.

Table 2. Porosity characteristics in the tip of fluidity tests

	Pore Area Fraction (%)	Pore per mm2	Average equivalent circular diameter (µm)	Max. equivalent circular diameter (µm)	Average of max. pore length (µm)	Max. pore length (µm)
L00	3.81	1±0.07	196±105	644	240±112	920
L25	3.57	1.5±0.03	161±65	389	192±69	419
L50	2.92	1.5±0.22	145±65	429	180±75	501

These results evidenced that for certain conditions, the techniques used for melt quality assessment might not be working under the specified assumptions. In the case of RPT, the layer of oxides found on the top of the samples for melt qualities L25 and L50 formed a solid layer upon solidification that acted as a lid, therefore partially isolating the rest of the sampled melt from the action of the reduced pressure, resulting in decreased unfurling of oxide films. Figure 22 schematically represents the proposed mechanism. In the present experiments, the use of RPT coupled with DI or BI analysis was uncappable of detecting the loss of quality due to the machining chips addition.

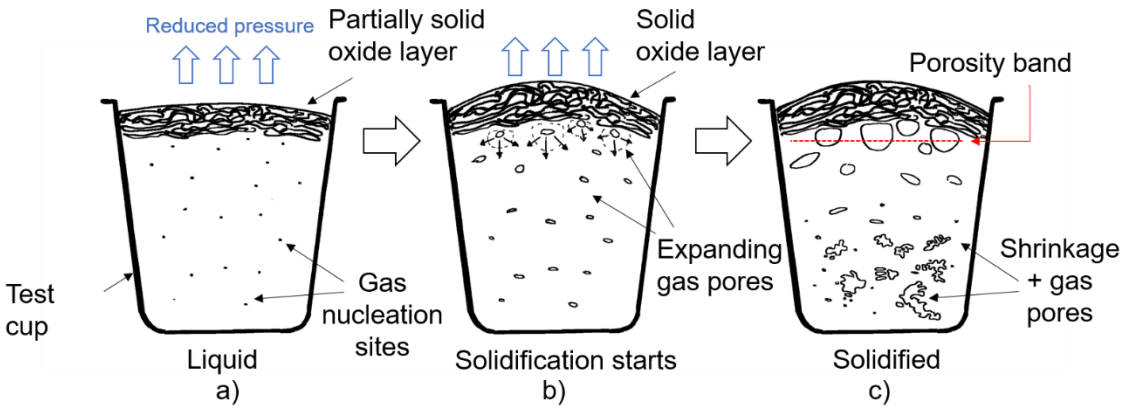

Figure 22. Schematic representation of the proposed mechanism for a solidifying RPT with a high level of oxides: a) sample before solidification start, b) start of solidification and c) solidified.

The measurement of melt quality with fluidity tests relies on correlating possible oxides with the change in fluidity. As big oxides were found on the top of the feeder, they did not take part in changing the fluidity. The observed values are then those of the base alloy, regardless of the melt quality. Smaller oxides and inclusions did flow with the bulk of the melt into the spiral. This is evidenced though the image analysis of the spirals tips. The decrease of average porosity length and pore area fraction, coupled with the increase in pore per mm^2 is most likely related to a higher number of nucleation sites for gas porosity. In the case of L50 melt quality, a compounded effect of increased nucleation sites, due to oxide content, coupled with the measured decrease in hydrogen levels (Figure 17a) resulted in a considerable decrease in pore area fraction.

A similar effect to that observed in fluidity tests can be attributed to the results for Prefil tests. As the melt is feed through the filter by the combined action of a pressure difference and gravity, oxides would only choke the flow though the filter after most of the melt is through.

3.2.2 Effect of melt quality on tensile properties

Producing the tensile samples through the tilting mould technique, a laminar flow is achieved. This, coupled with the correction of the chemical composition enables the assessment of the change in tensile properties as related solely to the melt quality.

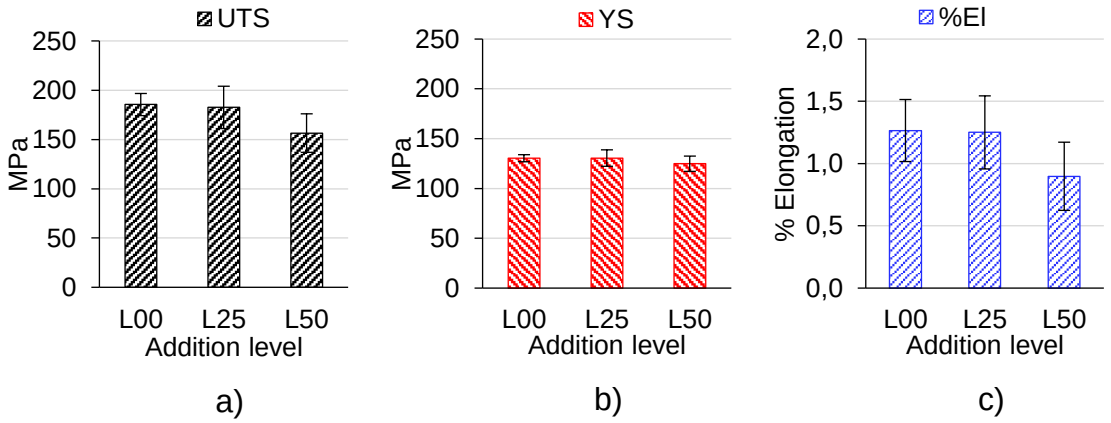

Figure 23. a) UTS, b) YS and c) %Elongation average values for the three melt quality levels tested. Error bars represent standard deviation.

Tensile test results are presented in Figure 23. Average values were seen to be virtually the same between L00 and L25 melt qualities. L50 machining chip additions resulted in a lower value of UTS and %elongation. Weibull distribution fitting for the analysis of scatter in values was performed for UTS and %elongation (Figure 24). Both L00 and L25 qualities showed a good fit to 2-parameter distributions for both UTS and %elongation. Only UTS values for L50 melt quality were found to fit Weibull distributions.

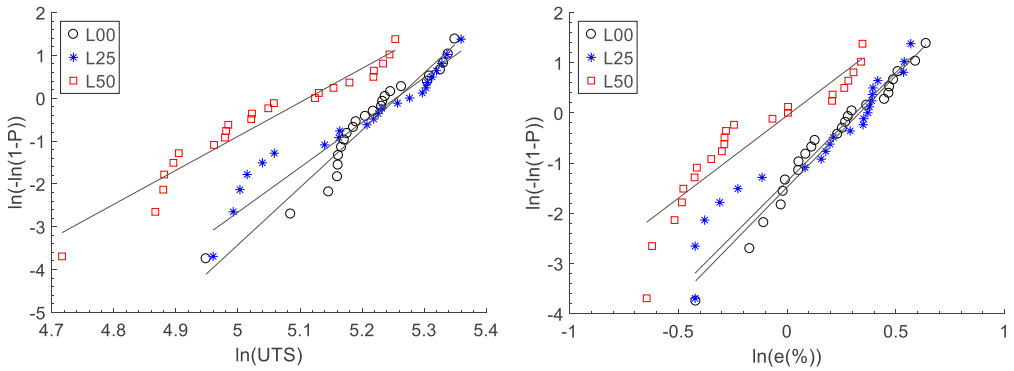

Figure 24. Weibull plots for a) UTS and b) %elongation for the three melt qualities tested.

Examination of the fracture surface of the tensile samples (Figure 25) revealed a transition from mostly shrinkage-type porosity for L00 melt quality samples towards mainly oxide films defects for L50 samples. L25 quality samples presented both shrinkage porosity as well as oxide films. Following the work of Cáceres and Selling [65], the UTS was correlated to the area fraction of defects determined from the projected area of the fracture surface (Figure 26 and Figure 27). It was observed that the UTS values decreased with increasing defect area fraction, regardless of the type of defect.

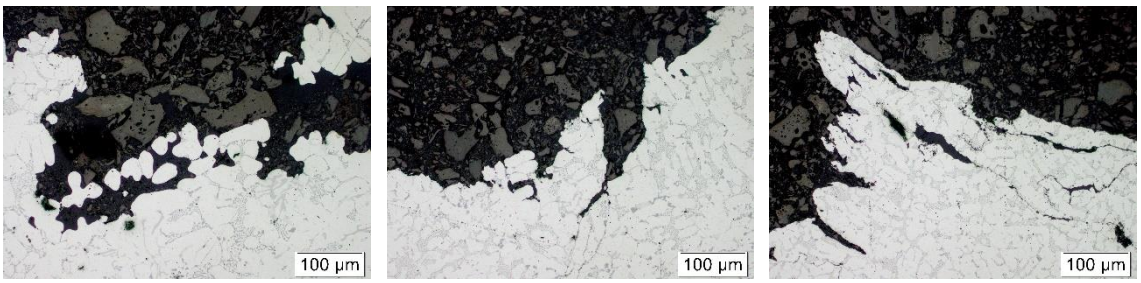

Figure 25. Typical tensile fracture profiles for the a) L00, b) L25 and c) L50 melt qualities tested.

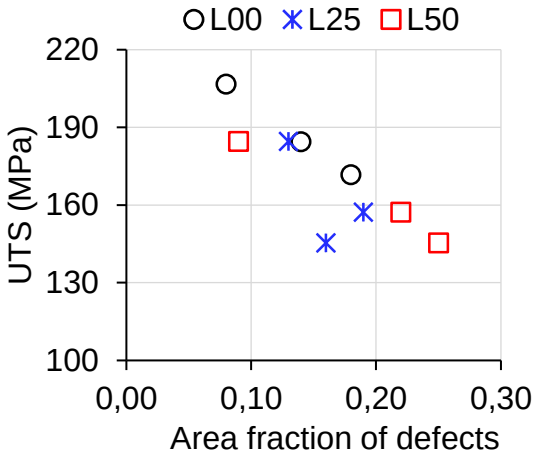

Figure 26. UTS vs Area fraction of defects for the three melt qualities tested.

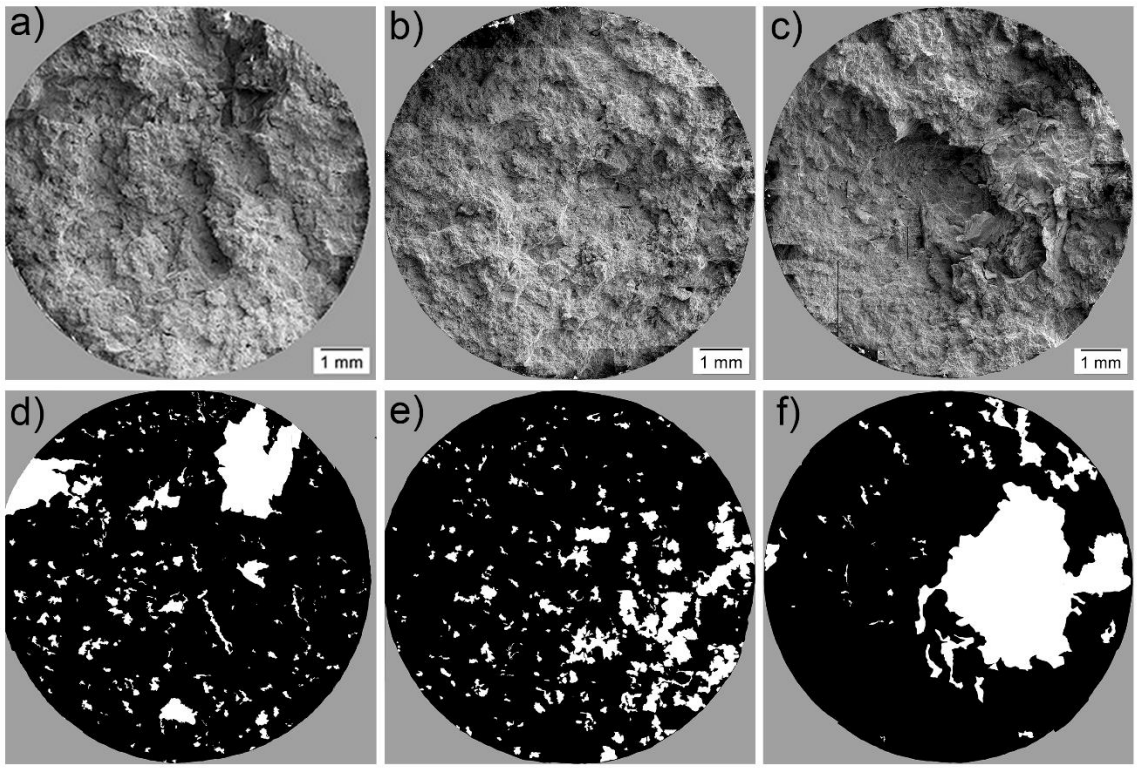

Figure 27. Typical tensile fracture surface for a) L00, b) L25 and c) L50 melt qualities and corresponding binary image of the defect areas characterization: d) L00, e) L25 and f) L50.

The average UTS, YS and % Elongation (as observed in Figure 23) did not show any change with the decrease of melt quality from L00 to L25. The Weibull analysis of the results (Figure 24) corroborated this observation. The scale parameter for L00 and L25 melt qualities was found to be the same for these two melt qualities (σ_0^{L00} = 192, σ_0^{L00} = 191). The main difference between the two qualities was observed to be related to the scatter in properties as represented by the shape parameter; with the L00 quality ensuing a lower scatter (m^{L00} = 13.37) compared to the L25 quality (m^{L25} = 10.47). The information given by the Weibull analysis was found to be in good agreement with the defect area fraction correlation to UTS values (Figure 26). As the decrease of melt quality is expected to increase the presence of defects in the microstructure, the scatter in the results will increase with lower melt qualities. In

Figure 26 this can be observed considering the defect fraction for each quality; the L00 melt quality yielded defect area fractions of 8 to 18%, L25 values between 13 and 19% and L50 from 9% to 25%.

3.3 GRAIN REFINEMENT & MODIFICATION

Supplements III & IV were aimed at clarifying the contradictory results observed in the literature with regards to grain refinement. The correlation of grain sizes to the corresponding effects in tensile properties was also approached.

Taking advantage of the directional solidification technique, samples from a clean melt with low level of defects and controlled cooling rates can be produced. The characterization of the resulting samples is presented first followed by the corresponding effects in tensile properties. Conditions with only Si modification (+Sr), only grain refinement (+GR) and with both (+Sr+GR) were produced. The reference alloy was an Al-10Si alloy with no further alloying elements to evaluate the sole effect of grain refinement and modification. Three cooling rates were produced and are referred to as SDAS 35, SDAS 15 and SDAS 6.

3.3.1 Characterization

3.3.1.1 Composition changes

The effect of remelting and subsequent directional solidification was evaluated from the point of view of possible settlement of particles and of composition variation in those conditions with grain refiner addition (+GR and +Sr+GR). The results of optical emission spectroscopy measurements along the gauge length of the different cooling rates are presented in Figure 28. Samples before remelting are referred to as "as-cast". A decrease of Ti and B content was observed for both +GR and +Sr+GR conditions for the three cooling rates tested. Further analysis by Energy Dispersive Spectrometry of the bottom of these bars revealed a band of Ti-rich particles. From the literature reviewed, these particles are most likely TiB_2 particles that have settled during the time for remelting and homogenization in the directional solidification equipment. The effect is more acute for the slower SDAS 35 cooling rate as the bar spent a considerably longer time in molten state if compared to the SDAS 15 and 6 cooling rates.

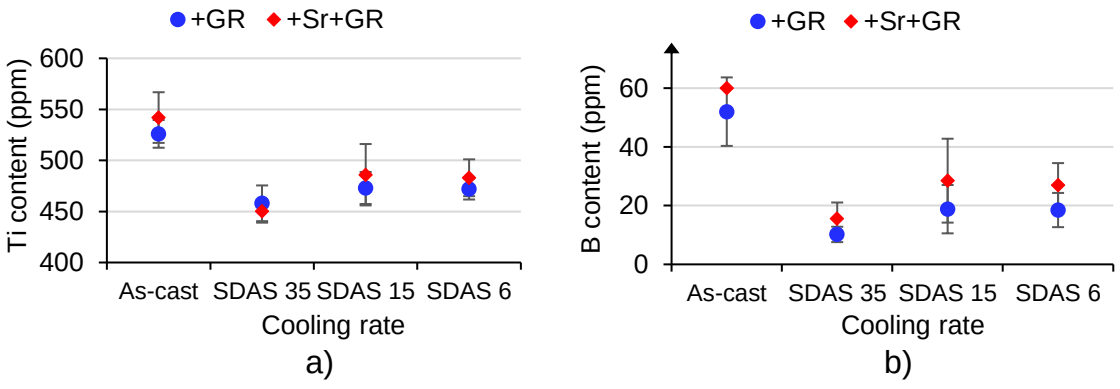

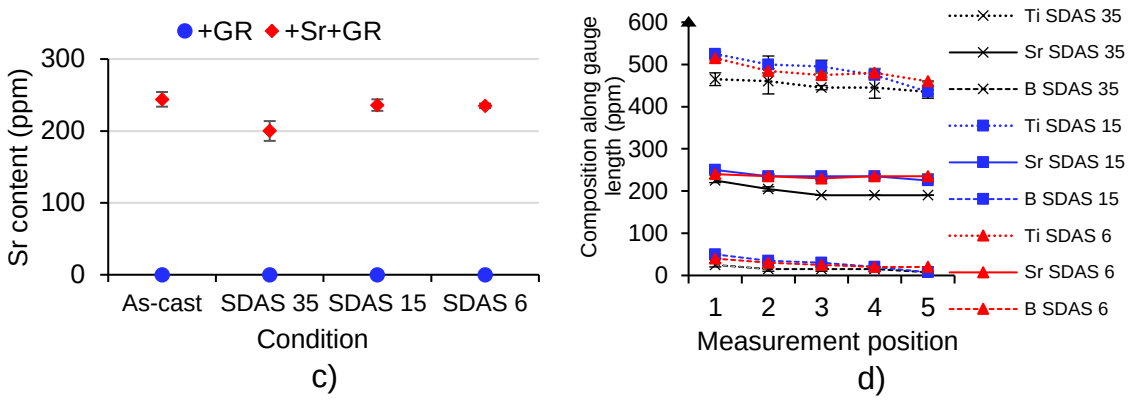

Figure 28. Average a) Ti, b) B and c) Sr content for +GR and +Sr+GR conditions. d) Variation of Ti, Sr and B along the gauge length for the three tested cooling rates in the +Sr+GR condition

3.3.1.2 Microstructure

The grains were characterized in both longitudinal and cross sections of the controlled cooling rate samples. Average grain size values are reported in Table 3. The reference Al-10Si and the +Sr conditions, as displayed in Figure 29, presented clearly columnar structures in the solidification direction for the SDAS 35 and 15 cooling rates. The fastest cooling rate (SDAS 6) displayed a mixed macrostructure with coexisting equiaxed and columnar grains. Increasing the cooling rate was found to decrease the column width. Without grain refiner addition, high cooling rates alone were not enough to produce equiaxed grain structures.

The condition with only grain refiner addition (+GR) consisted of coarse columnar grains for the SDAS 35 cooling rate. The SDAS 15 and 6 cooling rates resulted in equiaxed grains, with the fastest cooling rate (SDAS 6) producing the finest grain size. On the other hand, the combined addition of Si modifier and grain refiner (+Sr+GR) was found to produce equiaxed grains for all the cooling rates tested. The increase of cooling rate from SDAS 35 to SDAS 6 effected a slight decrease in grain size. Representative grain structures for the +GR and +Sr+GR are presented in Figure 30.

The composition measurements revealed a band of settled Ti-rich particles. Since the same concentrations of Ti and B and the same settling behaviour of TiB2 was observed for both alloys after remelting, the same amount of nucleant particles must be present for both alloys. With the solidification front progressing in the opposite direction of the settlement of particles, as the front advances, it could effectively promote some of the TiB_2 particles to be activated by the constitutional undercooling ahead of the front. The consequences of such events would be improved grain refinement and entrapment of particles that have not been successfully activated or pushed ahead of the solidification front.

Table 3 Grain sizes as function of condition and cooling rate. Column width is reported for columnar grains (marked with *)

Grain size (µm)	SDAS (µm)		
	35	15	6
Al-10Si	6926 ± 2577*	4061 ± 2138*	995 ± 195*
+Sr	3316 ± 1021*	2054 ± 788*	601 ± 761
+GR	4031 ± 1291*	275 ± 51	139 ± 25
+Sr+GR	304 ± 48	200 ± 43	138 ± 25

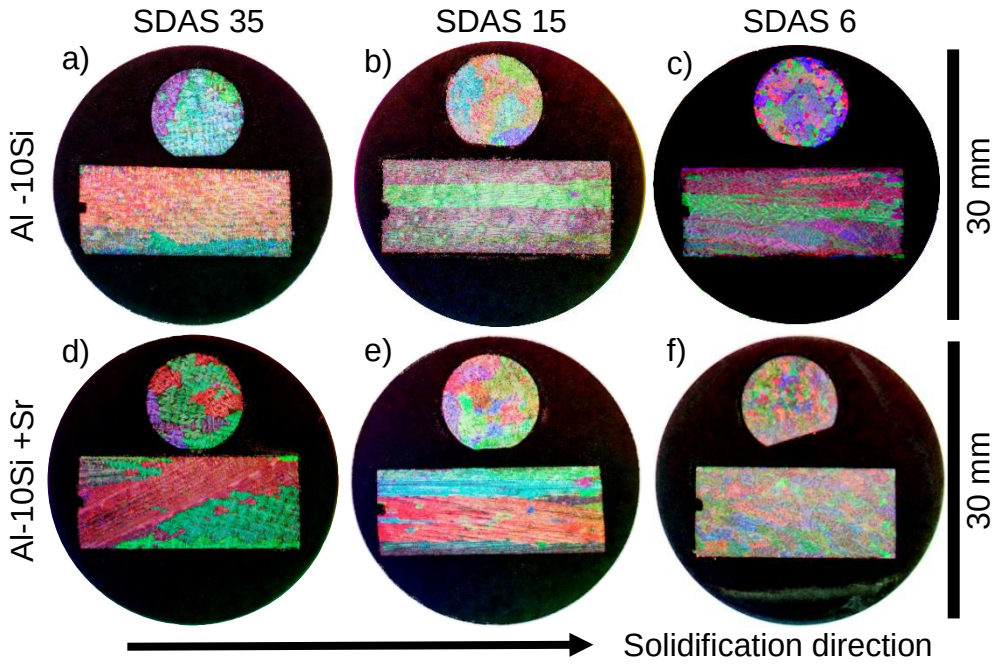

Figure 29. Macrographs of the cross and longitudinal section of a) SDAS 35, b) SDAS 15 and c) SDAS 6 cooling rates in Al-10Si alloy and d) SDAS 35, e) SDAS 15 and f) SDAS 6 cooling rates in the Al-10Si+Sr condition

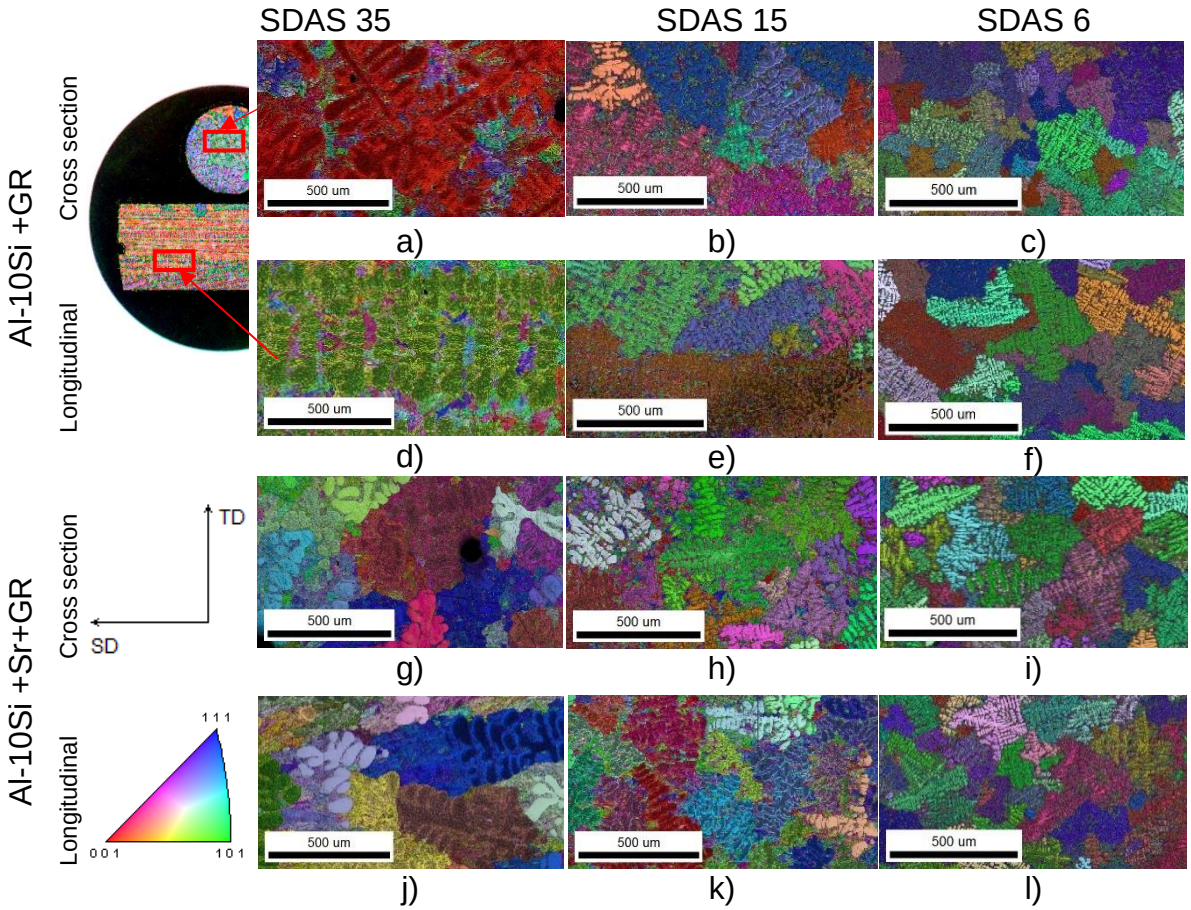

Figure 30. Inverse Pole Figure (IPF) maps of the three cooling rates tested for the Al-10Si+GR condition (a-f) and for the Al-10Si+Sr+GR condition (g-l).

The characteristic microstructures of the four tested conditions related to the different cooling rates are presented in Figure 31. Regardless of the condition,

increasing the cooling rate refined the eutectic Si. For the SDAS 6 cooling rate, the microstructure has reached a high level of refinement and the conditions without chemical modification have achieved a quench modified microstructure. The addition of Sr for modification of eutectic Si (+Sr and +Sr+GR conditions) successfully changed the Si morphology from the coarse, acicular Si shape found in unmodified alloys into homogeneously distributed fine fibrous Si particles. No change in the modification effect was observed with the combined addition of Al-10Sr and Al-5Ti-1B (+Sr+GR) compared to the sole addition of Sr (+Sr condition). A slight modification effect was noticed for the highest cooling rate (SDAS 6) of the grain refined only alloy (+GR) when compared to the reference Al-10Si alloy.

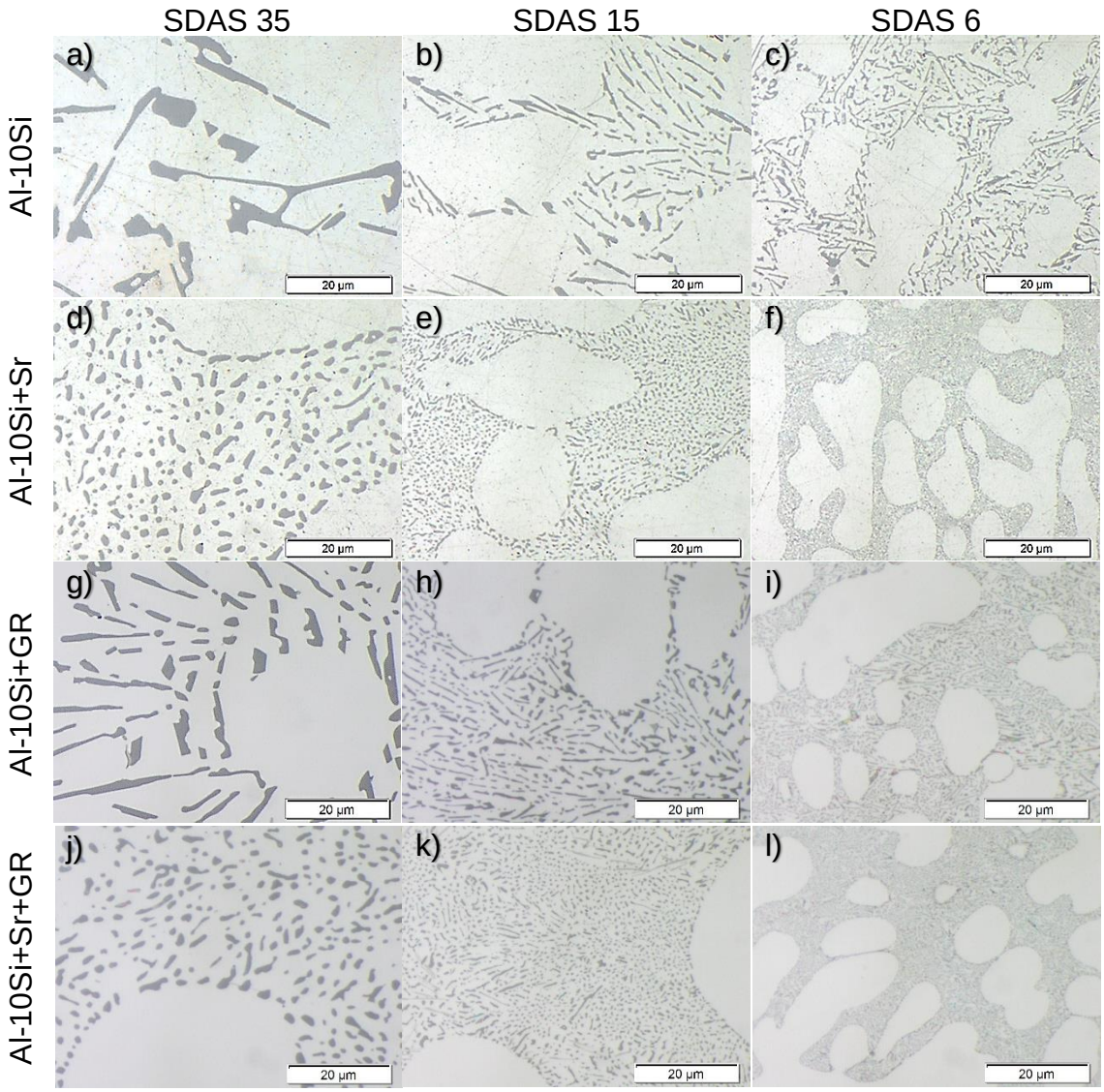

Figure 31. Representative microstructures of the three cooling rates tested for (a-c) Al-10Si, (d-f) Al-10Si+Sr, (g-i) Al-10Si+GR and (j-l) Al-10Si+Sr+GR.

3.3.2 Effects on tensile properties

The effect of the various cooling rates and additions on the tensile properties is presented in Figure 32. As has been previously observed, the increase in cooling rate improved the ultimate tensile strength (UTS) and the yield strength (YS) in all the

conditions tested. On the other hand, the elongation values presented different trends: the reference Al-10Si alloy, with Si particle length decreasing with the increasing cooling rate displayed an improvement in the elongation. The alloys with Sr for modification (+Sr and +Sr+GR) presented the opposite trend; the increase in cooling rate resulted in a decrease in elongation which is probably related to the interaction between dendrite size and the eutectic Si particles as previously proposed by Wang and Cáceres [66]. No clear trend was observed for the condition with only grain refiner addition (+GR). Overall, the elongation values are higher than those that can be expected in conventional die casting processes due to the lower level of defects expected. This has also been reported by Drar and Svensson [67]

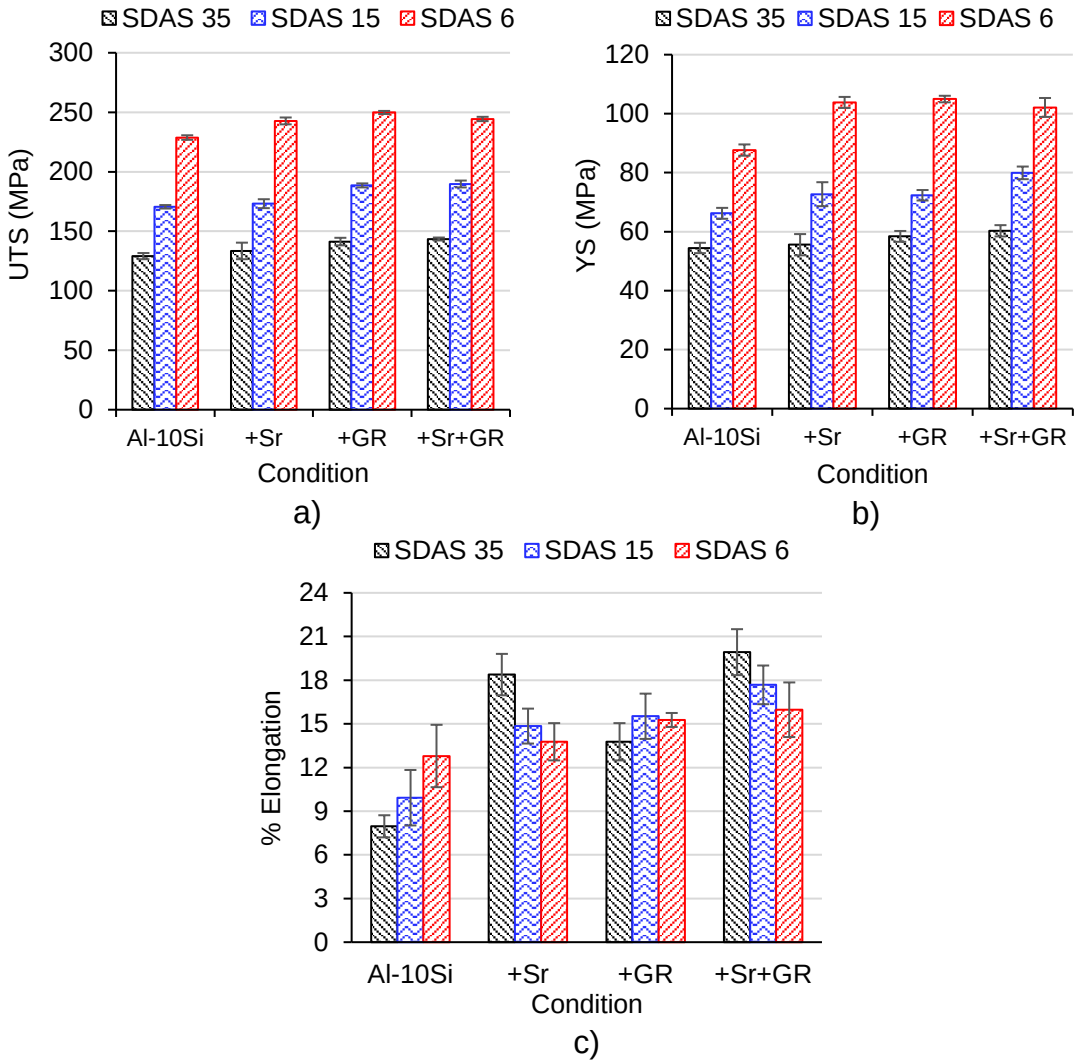

Figure 32. a) UTS, b) YS and c) %elongation as a function of cooling rate and condition.

3.3.2.1 Slow cooling rate (SDAS 35)

At the slowest cooling rates, compared to the reference Al-10Si alloy, while no change in UTS or YS was observed, a 130% increase in elongation was achieved with the addition of Sr (+Sr condition). This was due to the change from a flake-like Si morphology to a modified fibrous one. Both Al-10Si reference alloy and the +GR condition displayed columnar grains and an unmodified Si microstructure. Even so, the % elongation was noticeably higher for the +GR condition. UTS and YS were also

improved. The combined addition of Al-10Sr and Al-5Ti-1B resulted in the highest UTS, YS and % elongation values. The level of improvement observed was almost additive for the UTS and YS values.

3.3.2.2 Medium cooling rate (SDAS 15)

At this cooling rate by modification of eutectic Si (+Sr) raised the YS of the alloy in 10% and the elongation in 50% with respect to the reference alloy. The addition of grain refiner resulted in equal improvements of YS and elongation plus a 9% improvement in UTS. As both the reference alloy and the +Sr condition had a columnar grain structure while the +GR condition had equiaxed grains (275 ± 51 µm), the improvement observed for the grain refined samples could be due to more homogeneously distributed micro-defects. The highest improvement for the combined addition of modifier and grain refiner was observed at this cooling rate. With a grain size (200 ± 43 µm) similar to the grain refined only condition, the improvement can be related to the modification of the eutectic Si.

3.3.2.3 Fast cooling rate (SDAS 6)

For this cooling rate, there was no relevant change in % elongation. A small UTS increase (6%) and 18% increase in YS were achieved by Sr addition (+Sr condition). The behaviour of +GR and +Sr+GR conditions was virtually the same as observed for +Sr. As the eutectic Si size has become rather small, the detrimental effect of the flake-like morphology is reduced and the elongation values are similar for both modified and un-modified alloys. For such cooling rates (comparable to HPDC process) the addition of modifiers might be beneficial for improvement of YS.

3.3.2.4 Grain size or SDAS

To further analyse the influence of grain size and SDAS in tensile properties, Hall-Petch equations were fitted with the tensile results for the +Sr+GR condition. The corresponding results are plotted in Figure 33.

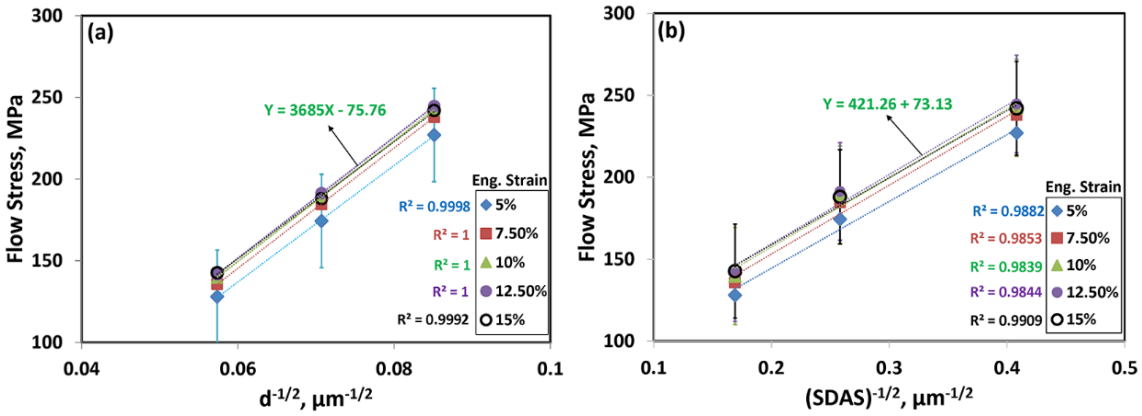

Figure 33. Flow stress vs inverse square root of a) grain size and b) SDAS plots for the Al-10Si+Sr+GR condition.

With R^2 values near unity for both fittings, a good linear relationship was found for both grain size and SDAS. When considering the grain size, the calculated resistance of the lattice to dislocation motion (σ_0) would be negative, which would be

meaningless from a physical perspective. The values for the SDAS fitting were however more reasonable, with values between 65 and 79 MPa for σ_0 and 390 to 420 MPa $\mu m^{-1/2}$ for the strengthening coefficient (k), which were similar to those previously observed in the literature [68].

3.3.2.5 Fracture characterization

The fracture mechanisms were investigated ex- and in-situ. Fracture profile micrographs for the different cooling rates and conditions tested can be observed in Figure 34. The crack propagated following the longitudinal direction of the eutectic Si flakes for the unmodified alloys (Al-10Si and Al-10Si+GR) and through the dendrite/eutectic interface occasionally traversing the α-Al dendrites in the modified alloys (Al-10Si+Sr and +Sr+GR). Secondary cracks were observed for all the cooling rates in unmodified alloys and for SDAS 35 and 15 cooling rates for the modified alloys.

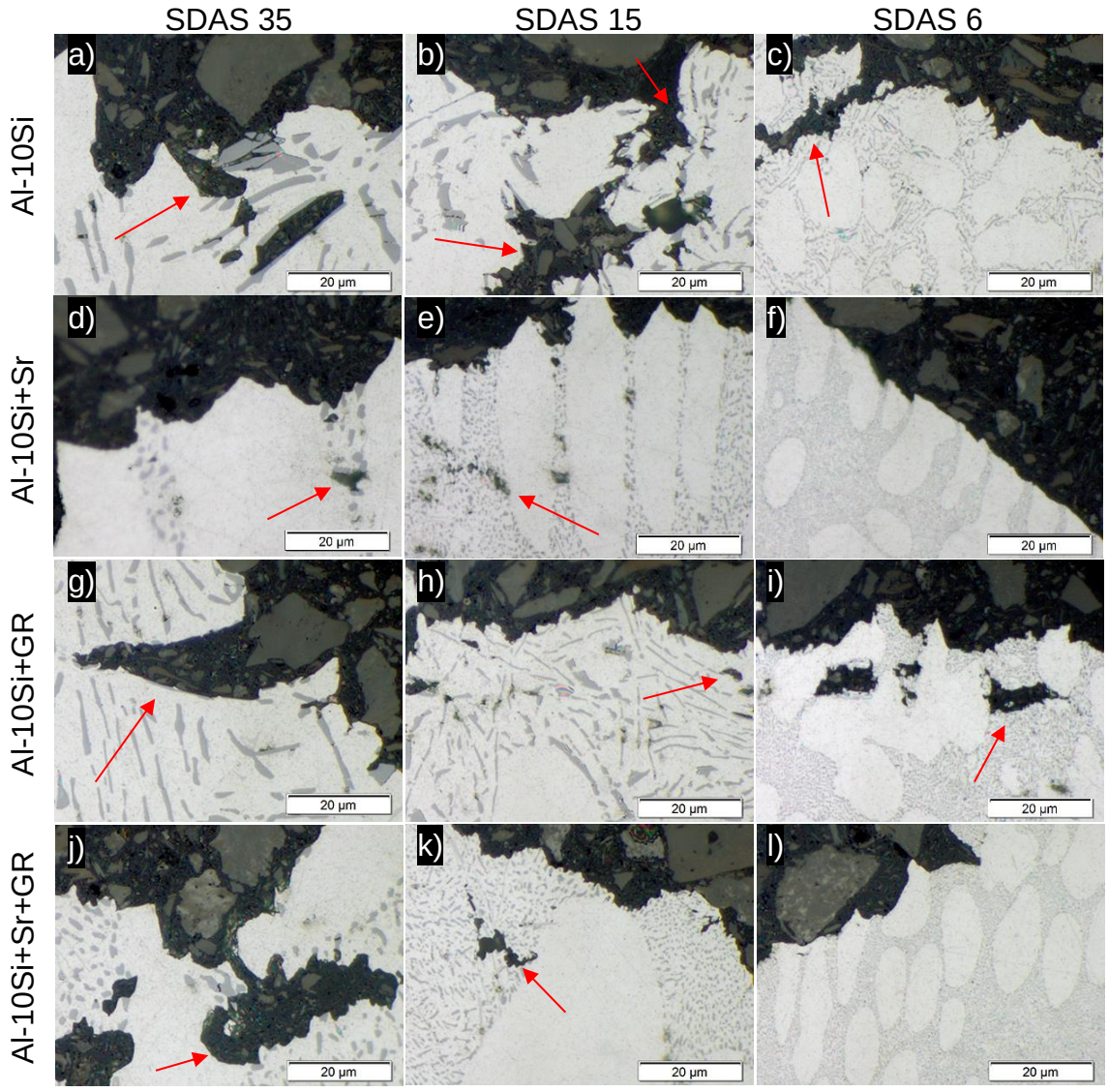

Figure 34. Typical fracture profiles for the three cooling rates tested: (a-c) Al-10Si alloy, (d-f) Al-10Si+Sr, (g-i) Al-10Si+GR and (j-l) Al-10Si+Sr+GR. Arrows mark secondary cracks.

For the highest cooling rate tested (SDAS 6), the finer microstructure, especially in terms of Si particle length for the unmodified alloys meant that although the crack would still propagate preferentially along the longitudinal direction of the flaky Si, this length had effectively become so short that the fracture profile was similar to that of the modified alloys.

In-situ tensile tests of the Sr-modified and grain refined condition (+Sr+GR) confirmed the ex-situ observations of the crack initiation location. As shown in Figure 35, visible cracks started to appear at 155 MPa in the region of study at the dendrite/eutectic boundary. Only one out of 15 initiated cracks was located at the grain boundary (Figure 35 c and d).

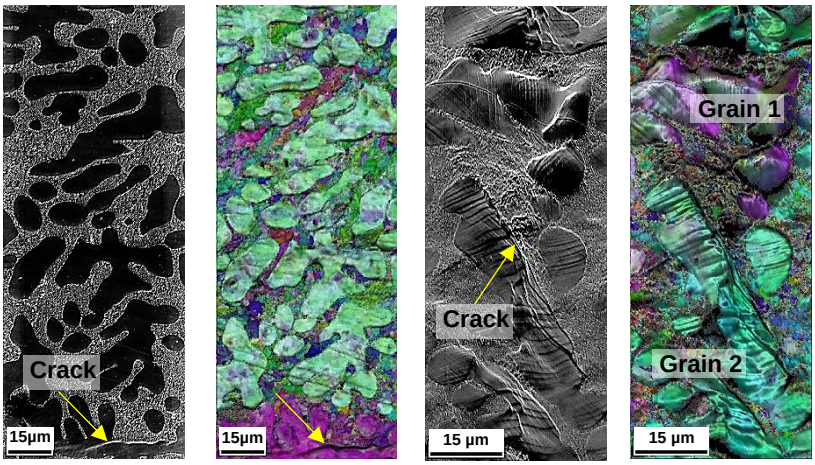

Figure 35. Crack initiation location in Al-10Si+Sr+GR alloy, SDAS 15. a) SEM micrograph and b) corresponding IPF map taken at 155 MPa. c) SEM micrograph and d) corresponding IPF map for the only crack found initiating on a grain boundary. Slip bands can clearly be seen inside the α-Al dendrites in c).

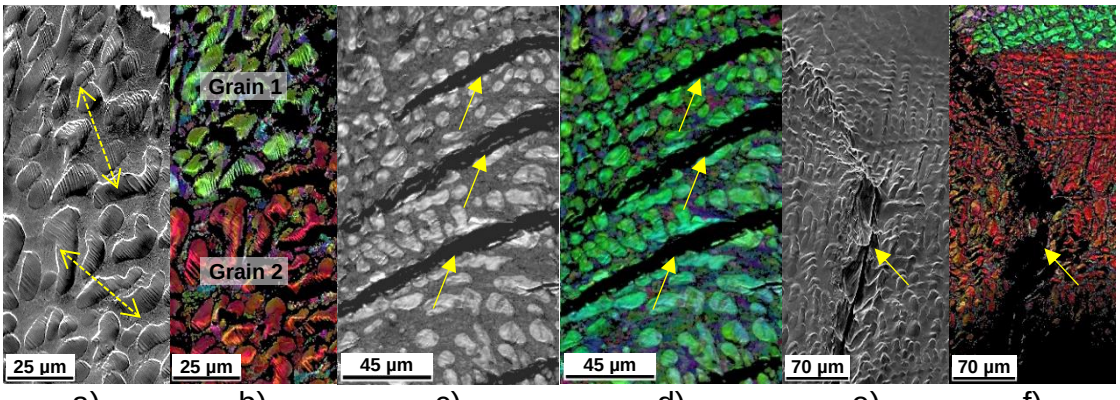

Figure 36. a) SEM micrograph and b) corresponding IPF map of two different grains with identical slip bands. c) SEM micrograph and d) corresponding IPF map of a series of cracks initiated and propagated within a grain. e) SEM micrograph and f) IPF map of a trans-granular crack after the fracture.

Slip bands appeared inside the α-Al dendrites during plastic deformation. As each grain was shown to activate an identical slip system (Figure 36 a and b), meaning that finer grains lead to more active slip systems, slightly improving the alloy plasticity. Cracks were observed to propagate in a trans-granular fashion as illustrated in Figure 36 c through f.

CHAPTER 4

CONCLUSIONS

In this chapter, the conclusions from the present work are presented.

State of the art knowledge and practices regarding the effect of system, process, and post-process variables have been applied to achieve setup properties. It was corroborated that by appropriate selection of the mentioned variables, a sand cast EN AC-42100 alloy can be T5 treated to achieve tensile and fatigue properties representative of an EN AC-46000 HPDC cast component. Also:

- For the EN AC 42100 alloy, the sand casting process provides superior tensile and fatigue properties compared to the plaster casting process.
- Fatigue properties for the sand cast EN AC 42100 alloy did not change with a T5 heat treatment or the addition of 2 wt. % of Cu.

The determination of the effect on tensile properties of three different known melt qualities as measured by different melt quality tests revealed that the available techniques for assessment of melt quality are inadequate. Further analysis is required to correctly interpret the results yielded from the tests. In addition to that, it was concluded that:

- The working principle of reduced pressure, fluidity and prefil tests is affected by the floatation of oxides.
- Machining chips addition increased the number of nucleation sites for pore, resulting in a decrease of maximum pore size. Coupled with a decrease in hydrogen, a reduction of pore area fraction will take place.
- Average tensile strength and elongation did not decrease with addition of up to 25 wt.% machining chips. Levels of 50 wt.% addition noticeably did.
- Application of Weibull statistics will accurately describe the change in scatter of tensile properties due to a decreased melt quality.

Grain refinement and Si modification experiments were performed under three different controlled cooling rates. Their effect on tensile properties was determined. It can be concluded that:

- The microstructure of Al-10Si alloys will be refined by increasing cooling rates, but equiaxed grains will not be obtained without addition of grain refiner.
- Additions of only Al-5Ti-1B grain refiner with low cooling rates corresponding to a SDAS value of 35 μm or higher will not produce an equiaxed structure. With the same cooling rate, combined grain refiner and Al-10Sr master alloy additions equiaxed grain structures can be achieved.
- Higher cooling rates will effectively produce equiaxed grains in the same size ranges with additions of only grain refiner as well as with combined Al-5Ti-1B and Al-10Sr.

- Improvements of UTS, YS and elongation beyond what was achieved by independent additions can be achieved by combined additions of Al-5Ti-1B with Al-10Sr master alloys in cooling rates corresponding to dendrite arm spacings of 15 μm and slower.
- Grain size does not have a meaningful relationship with flow stress through the traditional Hall-Petch equation.
- The first cracks in the area of study began within the plastic deformation region, between the Yield point and Ultimate Tensile Strength of the material at the dendrite/eutectic boundary, regardless of the grain boundary location and propagated through the grains, as trans-granular cracks.
- Slip bands appeared in the α-Al dendrites highlighting the role of the Al matrix in the overall mechanical properties of Al-Si alloys. Each grain contained an identical slip band direction, implying the indirect and possibly slight effect of grain size on the plasticity of Al-Si cast alloys.

CHAPTER 5

FUTURE WORK

CHAPTER INTRODUCTION

In this chapter, ideas based on the current work for continuing the development of high performing cast aluminium alloys are presented.

There are various routes that can be followed from the presented work.

Melt quality

If high performing cast components are to be produced, solutions to unequivocally determine the melt quality need to be developed. Furthermore, once the melt quality can be properly characterized in a timely manner, how to ensure a clean melt and how to improve the cleanliness of a low-quality melt is of interest.

Dynamic loading

The role of melt qualities and the interactive effect of grain size, eutectic modification and solidification rate has been presented in relation to static properties. As cast components undergo dynamic loading while on service. Most component failures during service can be related to such loading conditions. It is therefore relevant to evaluate those microstructural configurations favourable under static loading in terms of dynamic loads such as fatigue tests.

Elevated temperature applications

Based on the developed understanding on the importance of controlling the different steps in the production cycle, the performance of cast aluminium components needs to be extended to elevated temperatures. Literature suggests that certain alloying elements produce certain phases, that if present in the right amount and morphology, could produce the adequate strengthening. The processing route and the applied post-processes are believed to be a key element

REFERENCES

1. Major, F. and D. Apelian. *A Micro structural Atlas of Common Commercial Al-Si-X Structural Castings*. in *AFS Aluminum Structural Casting Conference*. 2003. Orlando, FL: AFS.
2. Warmuzek, M., *Aluminum-Silicon Casting Alloys. Atlas of Microfractographs*. 2004: ASM International.
3. Wang, L., M. Makhlouf, and D. Apelian, *Aluminum die casting alloys: Alloy composition, microstructure, and properties-performance relationships.* International Materials Reviews, 1995. **40**(6): p. 221-238.
4. Samuel, F.H., et al., *Effect of Mg and Sr additions on the formation of intermetallics in Al-6 Wt pct Si-3.5 Wt pct Cu-(0.45) to (0.8) Wt pct Fe 319-type alloys.* Metallurgical and Materials Transactions A, 1998. **29**(12): p. 2871-2884.
5. Sjölander, E. and S. Seifeddine, *The heat treatment of Al–Si–Cu–Mg casting alloys.* Journal of Materials Processing Technology, 2010. **210**(10): p. 1249-1259.
6. Cáceres, C.H., I.L. Svensson, and J.A. Taylor, *Strength-ductility behaviour of Al-Si-Cu-Mg casting alloys in T6 temper.* International Journal of Cast Metals Research, 2003. **15**(5): p. 531-543.
7. Seifeddine, S., *Characteristics of cast aluminium-silicon alloys: microstructures and mechanical properties*, in *Department of Mechanical Engineering / Component Technology - Castings*. 2006, Jönköping University: School of Engineering.
8. Shabestari, S.G. and H. Moemeni, *Effect of copper and solidification conditions on the microstructure and mechanical properties of Al–Si–Mg alloys.* Journal of Materials Processing Technology, 2004. **153-154**: p. 193-198.
9. Liu, L., et al., *Precipitation of β-Al5FeSi Phase Platelets in Al-Si Based Casting Alloys.* Metallurgical and Materials Transactions A, 2009. **40**(10): p. 2457-2469.
10. Taylor, J.A., *Iron-Containing Intermetallic Phases in Al-Si Based Casting Alloys.* Procedia Materials Science, 2012. **1**: p. 19-33.
11. Hwang, J.Y., H.W. Doty, and M.J. Kaufman, *The effects of Mn additions on the microstructure and mechanical properties of Al-Si-Cu casting alloys.* Materials Science and Engineering A, 2008. **488**(1-2): p. 496-504.
12. Gruzleski, J.E., B.M. Closset, and A.F.s. Society, *The Treatment of Liquid Aluminum-silicon Alloys*. 1990: American Foundrymen's Society, Incorporated.
13. Qiyang, L., L. Qingchun, and L. Qifu, *Modification of Al-Si alloys with sodium.* Acta metallurgica et materialia, 1991. **39**(11): p. 2497-2502.
14. Lu, S.Z. and A. Hellawell, *The mechanism of silicon modification in aluminum-silicon alloys: impurity induced twinning.* Metallurgical and Materials Transactions A, 1987. **18**(10): p. 1721-1733.
15. Makhlouf, M. and H. Guthy, *The aluminum-silicon eutectic reaction: mechanisms and crystallography.* Journal of Light Metals, 2001. **1**(4): p. 199-218.
16. Timpel, M., et al., *The role of strontium in modifying aluminium–silicon alloys.* Acta Materialia, 2012. **60**(9): p. 3920-3928.

17. Hegde, S. and K.N. Prabhu, *Modification of eutectic silicon in Al-Si alloys.* Journal of Materials Science, 2008. **43**(9): p. 3009-3027.
18. Mohanty, P.S. and J.E. Gruzleski, *Mechanism of grain refinement in aluminium.* Acta Metallurgica et Materialia, 1995. **43**(5): p. 2001-2012.
19. Lu, L. and A.K. Dahle, *Effects of combined additions of Sr and AlTiB grain refiners in hypoeutectic Al-Si foundry alloys.* Materials Science and Engineering A, 2006. **435-436**: p. 288-296.
20. Easton, M. and D. Stjohn, *Grain refinement of aluminum alloys: Part I. the nucleant and solute paradigms—a review of the literature.* Metallurgical and Materials Transactions A, 1999. **30**(6): p. 1613-1623.
21. Easton, M.A., et al., *Recent advances in grain refinement of light metals and alloys.* Current Opinion in Solid State and Materials Science, 2016. **20**(1): p. 13-24.
22. Mohanty, P.S. and J.E. Gruzleski, *Grain refinement mechanisms of hypoeutectic Al-Si alloys.* Acta Materialia, 1996. **44**(9): p. 3749-3760.
23. Spittle, J.A., *Grain refinement in shape casting of aluminium alloys.* International Journal of Cast Metals Research, 2006. **19**(4): p. 210-222.
24. Easton, M. and D. StJohn, *Grain refinement of aluminum alloys: Part II. Confirmation of, and a mechanism for, the solute paradigm.* Metallurgical and Materials Transactions A, 1999. **30**(6): p. 1625-1633.
25. StJohn, D.H., et al., *The Interdependence Theory: The relationship between grain formation and nucleant selection.* Acta Materialia, 2011. **59**(12): p. 4907-4921.
26. Vinod Kumar, G.S., B.S. Murty, and M. Chakraborty, *Settling behaviour of TiAl3, TiB2, TiC and AlB2 particles in liquid Al during grain refinement.* International Journal of Cast Metals Research, 2010. **23**(4): p. 193-204.
27. Lee, Y.C., et al., *The effect of grain refinement and silicon content on grain formation in hypoeutectic Al–Si alloys.* Materials Science and Engineering: A, 1999. **259**(1): p. 43-52.
28. Abdel-Reihim, M., et al., *Effect of solute content on the grain refinement of binary alloys.* Journal of Materials Science, 1987. **22**(1): p. 213-218.
29. Johnsson, M., *Grain refinement of aluminium studied by use of a thermal analytical technique.* Thermochimica acta, 1995. **256**(1): p. 107-121.
30. Qiu, D., et al., *A mechanism for the poisoning effect of silicon on the grain refinement of Al-Si alloys.* Acta Materialia, 2007. **55**(4): p. 1447-1456.
31. Prasad, A., et al., *Real-time synchrotron x-ray observations of equiaxed solidification of aluminium alloys and implications for modelling.* IOP Conference Series: Materials Science and Engineering, 2015. **84**(1): p. 012014.
32. Greer, A.L., et al., *Grain Refinement of Aluminium Alloys by Inoculation.* Advanced Engineering Materials, 2003. **5**(1-2): p. 81-91.
33. Chen, Z., et al., *Grain refinement and tensile properties improvement of aluminum foundry alloys by inoculation with Al–B master alloy.* Materials Science and Engineering: A, 2012. **553**: p. 32-36.
34. Chen, Z., et al., *Grain refinement of hypoeutectic Al-Si alloys with B.* Acta Materialia, 2016. **120**: p. 168-178.
35. Birol, Y., *AlB3 master alloy to grain refine AlSi10Mg and AlSi12Cu aluminium foundry alloys.* Journal of Alloys and Compounds, 2012. **513**: p. 150-153.
36. Birol, Y., *Performance of Al-5Ti-1B and Al-3B grain refiners in investment casting of AlSi7Mg0·3 alloy with preheated ceramic moulds.* International Journal of Cast Metals Research, 2012. **25**(5): p. 296-300.

37. Liao, H. and G. Sun, *Mutual poisoning effect between Sr and B in Al–Si casting alloys.* Scripta Materialia, 2003. **48**(8): p. 1035-1039.
38. Samuel, E., et al., *Effect of grain refiner on the tensile and impact properties of Al–Si–Mg cast alloys.* Materials & Design, 2014. **56**: p. 468-479.
39. Sigworth, G., *Understanding quality in aluminum castings.* International Journal of Metalcasting, 2011. **5**(1): p. 7-22.
40. Campbell, J., Castings. 2003: Butterworth-Heinemann.
41. Di Sabatino, M., S. Akhtar, and L. Arnberg, *State-of-the-art characterization tools for Al foundry alloys.* Metallurgical Science and Tecnology, 2013. **30**(1).
42. Hudson, S. and D. Apelian, *Clean Aluminum Processing: New Avenues for Measurement and Analysis.* Light Metals 2014, 2014: p. 1025-1029.
43. Poynton, S., M. Brandt, and J. Grandfield. *A review of inclusion detection methods in molten aluminium*. in *Light Metals*. 2009. John Wiley & Sons.
44. Đurđević, M.B., Z. Odanović, and J. Pavlović-Krstić, *Melt quality control at aluminum casting plants.* Metalurgija, 2010. **16**(1): p. 63-76.
45. Dispinar, D. and J. Campbell, *Critical assessment of reduced pressure test. Part 1: Porosity phenomena.* International Journal of Cast Metals Research, 2004. **17**(5): p. 280-286.
46. Timelli, G. and F. Bonollo, *Fluidity of aluminium die castings alloy.* International Journal of Cast Metals Research, 2007. **20**(6): p. 304-311.
47. Simard, A.A., et al., *Cleanliness measurement benchmarks of aluminum alloys obtained directly at-line using the prefil-footprinter instrument.* Light Metals, 2000: p. 739-744.
48. Dispinar, D. and J. Campbell. *A comparison of methods used to assess aluminium melt quality*. in *TMS Annual Meeting*. 2007.
49. Stanică, C. and P. Moldovan, *Aluminum melt cleanliness performance evaluation using PoDFA (porous disk filtration apparatus) technology.* UPB Scientific Bulletin, Series B: Chemistry and Materials Science, 2009. **71**(4): p. 107-114.
50. Enright, P., et al., *Characterisation of molten metal quality using the pressure filtration technique.* 2003.
51. Totten, G.E. and D.S. MacKenzie, *Handbook of Aluminum: Vol. 1: Physical Metallurgy and Processes*. 2003: CRC Press.
52. Fredriksson, H. and U. Åkerlind, *Faceted and Dendritic Solidification Structures*, in *Solidification and Crystallization Processing in Metals and Alloys*. 2012, John Wiley & Sons, Ltd. p. 475-586.
53. Easton, M., C. Davidson, and D. St John, *Effect of Alloy Composition on the Dendrite Arm Spacing of Multicomponent Aluminum Alloys.* Metallurgical and Materials Transactions A, 2010. **41**(6): p. 1528-1538.
54. Sigworth, G.K., *Fundamentals of solidification in aluminum castings.* International Journal of Metalcasting, 2014. **8**(I).
55. Beeley, P., *Foundry technology*. 2001: Butterworth-Heinemann.
56. Taylor, J.A., et al., *An empirical analysis of trends in mechanical properties of T6 heat treated Al-Si-Mg casting alloys.* International Journal of Cast Metals Research, 2000. **12**(6): p. 419-430.
57. Sjölander, E., *Heat treatment of Al-Si-Cu-Mg casting alloys,*, in *JTH. Research area Materials and manufacturing – Casting, Jönköping University*. 2011, Chalmers Reproservice: Göteborg.
58. Dispinar, D. and J. Campbell, *Use of bifilm index as an assessment of liquid metal quality.* International Journal of Cast Metals Research, 2006. **19**(1): p. 5-17.

59. Kori, S.A., B.S. Murty, and M. Chakraborty, *Development of an efficient grain refiner for Al–7Si alloy and its modification with strontium.* Materials Science and Engineering: A, 2000. **283**(1–2): p. 94-104.
60. Basavakumar, K.G., P.G. Mukunda, and M. Chakraborty, *Influence of grain refinement and modification on microstructure and mechanical properties of Al–7Si and Al–7Si–2.5Cu cast alloys.* Materials Characterization, 2008. **59**(3): p. 283-289.
61. Birol, Y., *Impact of grain size on mechanical properties of AlSi7Mg0.3 alloy.* Materials Science and Engineering: A, 2013. **559**: p. 394-400.
62. Williamson, K., *Research methods for students, academics and professionals: Information management and systems*. 2002: Elsevier.
63. Tiryakioğlu, M. and D. Hudak, *Guidelines for two-parameter weibull analysis for flaw-containing materials.* Metallurgical and Materials Transactions B: Process Metallurgy and Materials Processing Science, 2011. **42**(6): p. 1130-1135.
64. *Premetz Analysis*. Accessed 2017-08-02; Available from: https://premetz.com/pages/analysis.
65. Cáceres, C.H. and B.I. Selling, *Casting defects and the tensile properties of an AlSiMg alloy.* Materials Science and Engineering: A, 1996. **220**(1): p. 109-116.
66. Wang, Q.G. and C.H. Cáceres, *The fracture mode in Al-Si-Mg casting alloys.* Materials Science and Engineering A, 1998. **241**(1-2): p. 72-82.
67. Drar, H. and I.L. Svensson, *Characterization of tensile properties and microstructures in directionally solidified Al-Si alloys using linear roughness index.* Materials Characterization, 2006. **57**(4-5): p. 244-258.
68. Thangaraju, S., et al., *On the Estimation of True Hall–Petch Constants and Their Role on the Superposition Law Exponent in Al Alloys.* Advanced Engineering Materials, 2012. **14**(10): p. 6.

APPENDED PAPERS

Supplement I

M. Riestra, S. Seifeddine, E. Sjölander; Tailoring Al-7Si-0.3Mg Cast Alloy Properties to Represent HPDC Tensile and Fatigue Behaviour in Component Prototypes.

Presented in High Tech Die Casting 2016, June 22nd-23rd, Venice, Italy. Published in Metallurgia Italiana, Associazione Italiana di Metallurgia. (2016) **108**: pp. 33-36.

Supplement II

M. Riestra, A. Bjurenstedt, T. Bogdanoff, E. Ghassemali, S. Seiffedine; Complexities in the Assessment of Melt Quality.

Presented in MS&T17, Light Metals Technology 2017, October 8th-12th, Pittsburgh, Pennsylvania, USA. Published in International Journal of Metalcasting 2017, DOI 10.1007/s40962-017-0179-y.

Supplement III

M. Riestra, E. Ghassemali, T. Bogdanoff, S. Seifeddine; Interactive Effects of Grain Refinement, Eutectic Modification and Solidification Rate on Tensile Properties of Al-10Si Alloy.

Materials Science and Engineering: A, 2017. **703**: p. 270-279

Supplement IV

E. Ghassemali, M. Riestra, T. Bogdanoff, B.S. Kumar, S. Seifeddine; Hall-Petch Equation in a Hypoeutectic Al-Si Cast Alloy: Grain Size vs. Secondary Dendrite Arm Spacing.

To be published in Procedia Engineering